DESIGN AND ANALYSIS OF CIRCULAR DIFFRACTION GRATINGS

CONCEPTION ET ANALYSE DES RESEAUX DE DIFFRACTION CIRCULAIRE

A Thesis Submitted to the Division of Graduate Studies
of the Royal Military College of Canada
by

James Leibold
Captain

In Partial Fulfillment of the Requirements for the Degree of
Masters of Science

April, 2015

Acknowledgements

I would like to thank my supervisor Dr. Ribal Georges Sabat, for trusting me to work on his original idea and for all of his support and guidance.

I would also like to thank Mr. Peter Snell, for all of the hours he spent expertly machining and polishing the circular diffraction grating generators.

In addition, I would like to thank Dr. Olivier Lebel, for providing the azo-glass material required for the experiments.

I would like to express my thanks to Ms. Jennifer Snelgrove, for her help with the SEM imagery.

Finally I would like to thank my Dad for his all of his careful work editing the document.

Abstract

Circular diffraction gratings have been formed by a new holographic technique using a circular diffraction grating generator. This specially designed fixture consists of a mirror in the shape of the interior of a truncated cone that splits and redirects a beam of coherent and collimated light to form an interference pattern of concentric rings. The interference pattern can be directly inscribed in surface-relief on a thin film of azobenzene functionalized glass forming compound. The derived theory correctly predicts that the pitch of the resulting circular gratings can be controlled by altering the geometry of the mirrored fixture. The inscription optical geometry can be further modified by adding a focusing lens and by changing the position of the focal point of inscribing light with respect to the sample film, affecting the rate of change of the pitch. Ring gratings with a relatively smooth centre can be created by lowering the height of the mirrored fixture below a certain critical height. The interior and exterior radii, the grating pitch, and the rate of pitch change (or chirp) of the resulting circular gratings can therefore be controlled, adding additional flexibility to the manufacturing process. The result is a relatively large scale circular or ring grating, on the order of 1 cm diameter, that can be quickly and easily fabricated using common optical lab equipment to meet photonic applications specific requirements.

Résumé

Des réseaux de diffraction circulaires ont été formées par une technique holographique en utilisant un générateur des réseaux de diffraction circulaires. Cette monture, spécialement conçue, consiste d'un miroir en forme de l'intérieur d'un cône tronqué, qui divise et redirige un faisceau de lumière cohérente pour former un patron d'interférence d'anneaux concentriques. Le patron d'interférence peut être inscrit directement en réseau de surface sur un film d'un verre fonctionnalisé d'azobenzéne. La théorie dérivée prédit correctement que le pas des réseaux circulaires résultants peut être contrôlé en modifiant la géométrie de la monture d'inscription. La géométrie optique d'inscription peut être encore modifiée par l'ajout d'une lentille ainsi qu'en changeant la position du point focal du rayon d'inscription par rapport au échantillon, ce qui affecte le taux de variation du pas. Des réseaux en anneaux ayant un centre relativement lisse peuvent être créés en diminuant la hauteur de la monture au-dessous d'une certaine taille critique. Les rayons intérieur et extérieur, le pas du réseau, et le taux de changement du pas peuvent donc tous être contrôlés. Le résultat est un réseau circulaire relativement grand de l'ordre de 1 cm de diamètre, qui peut être rapidement et facilement fabriqué en utilisant des équipements communs dans les laboratoires d'optique, afin de répondre aux exigences spécifiques des applications photoniques.

Table of Contents

List of Tables

List of Figures

List of Abbreviations

2D – Two dimensional

3D – Three dimensional

AFM – Atomic Force Microscope

CDG – Circular Diffraction Grating Generator

DR-1 – Dispersed Red 1

EM - Electromagnetic

LED – Light Emitting Diode

SEM – Scanning Electron Microscope

SRG - Surface Relief Grating

List of Symbols

m : Integer value representing diffraction order

$\vec{E}$: Electric field vector

$\vec{B}$: Magnetic field vector

ε : electric permittivity

μ : magnetic permeability

ρ : charge density

$\vec{J}$: current density vector

ω : angular frequency ($\omega = 2\pi\nu$)

ν : frequency of light

$\vec{k}$: wave vector in the direction the wave is travelling whose magnitude is $\left|\vec{k}\right| = 2\pi / \lambda$

λ : wavelength of light

$\vec{r}$: position vector

φ : phase (in radians)

θ : CDG mirror angle

m : minor aperture radius of CDG

h : CDG height

t : difference between radii of CDG major and minor apertures

s : distance from sample film to focal point of the source

h_c : critical height of CDG where interfering light from the mirror strikes the centre of the circular SRG without crossing over to the opposite side

Λ : Grating pitch (distance between consecutive diffraction grating grooves)

δ : distance from centre of circular SRG

CHAPTER 1: INTRODUCTION

1.1 Definitions and Properties of Diffraction Gratings

A diffraction grating is an optical element with a periodic modulation in its optical properties. This periodic variation can affect the amplitude of incoming light by modulating the brightness of the output light. Alternatively, it can affect the phase of the light by varying the optical path length of the output beam. The result of a typical diffraction grating is that a mono-chromatic beam of light is split into multiple beams of different orders as illustrated in Figure 1.1. It will be seen in the theory section of this thesis that the angle of these beams is dependent on the grating spacing (also called pitch), as well as the incident angle and wavelength of the incoming light. As a result of this dependence on wavelength, a beam of polychromatic light can also be dispersed by a diffraction grating, creating spatial separation of the beam's spectral elements.

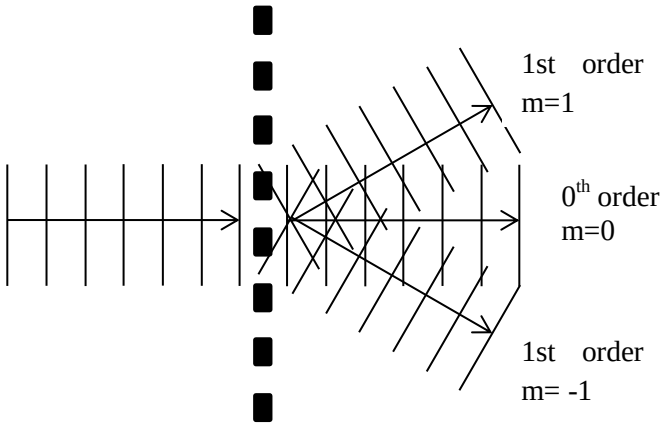

Figure 1.1 – An incoming beam of monochromatic light is split into different diffraction orders by a transmission amplitude grating. Additional orders are possible, such as m=2 and m=-2 but are not shown.

There are a wide range of types of diffraction gratings depending on how they are manufactured and what applications they are intended for. As already mentioned, if the grating variations are related to changes in the absorption, reflectance, or transmittance characteristics of the material, it is considered an amplitude grating because the grating will affect the amplitude of the light. If the modulation in the grating changes the index of

refraction in the material or changes the distance travelled in a material before an interface, it is called a phase grating because it is affecting the phase position of the light**.** Depending on whether the material used is transparent or reflective, a diffraction grating can be used as a transmission or reflection optical element. Diffraction gratings can have a constant pitch (meaning that the grating spacing is constant) or have a chirped pitch (meaning that the grating spacing changes over its surface). There are linear gratings whose structure is made of parallel straight lines as well circular gratings; which are formed in the shape of concentric circles.

Diffraction gratings may also have different profile shapes such as sinusoidal gratings**,** square wave also called binary gratings, triangle gratings, or saw-tooth patterns also known as blazed gratings as shown in Figure 1.2. The profile of the grating can affect the properties of the grating such as the diffraction efficiency. Diffraction efficiency is defined as the optical power from a diffraction order divided by the power from the incident light. Blazed gratings are sometimes used to increase the diffraction efficiency of one of the diffraction orders at the expense of the power of the other orders. For example, depending on the blaze angle and wavelength used, 1^{st} order diffraction efficiencies can range from 50% to approaching 100% efficiency in a blazed grating which is much higher than the maximum 1^{st} order efficiencies of 33.8% for sinusoidal gratings and 40.5% for square gratings[1].

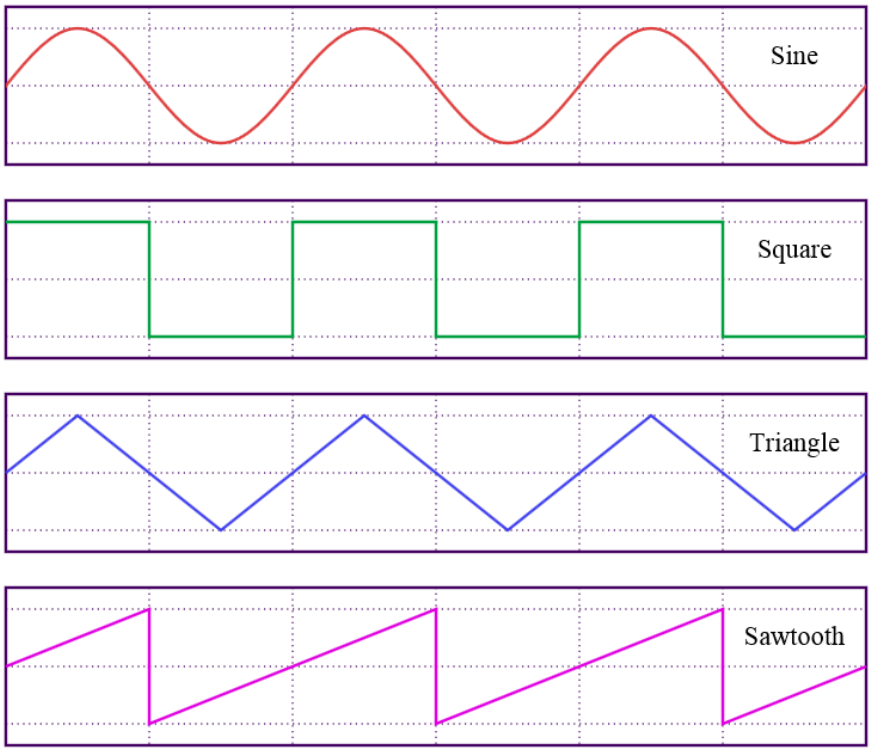

Figure 1.2 – Several examples of possible grating profiles. The profiles may represent changes in amplitude of the incoming light due to modulation of the reflectance or transmittance of the grating. The profiles may also represent the physical shape of the grating/air interface as for a surface relief grating (SRG) or changes in the index of refraction of the material in a volume phase grating.[a]

1.2 Early History of Diffraction Gratings

One of the earliest recorded examples of scientific observations of a diffraction grating was by James Gregory in 1673 when he proposed the experiment of shining a beam of light through a fine white feather[2]. David Rittenhouse is thought to have made the first man-made diffraction grating in 1785 using hair or thin wires evenly spaced across the threads of two parallel screws[3]. This type of grating can be classified as a linear, amplitude, transmission grating and is analogous to a multiple slit diffraction configuration. The hairs block light at a regular interval while the spaces in between the hairs act as slits. In 1821 Joseph von Fraunhofer rediscovered this technique[4] and developed the equation relating the angle of diffracted orders to the grating spacing and wavelength of light. Because of this and

[a] "Waveforms" by Omegatron - Own work. Licensed under Creative Commons Attribution-Share Alike 3.0-2.5-2.0-1.0 via Wikimedia Commons - http://commons.wikimedia.org/wiki/File:Waveforms.svg#mediaviewer/File:Waveforms.svg

his numerous contributions to the field of spectroscopy, the theory of far field diffraction was later named in his honour.

Works in the early 19th century by the famous French physicist Augustin-Jean Fresnel also contributed to the invention of a specialized circular diffraction grating called a Fresnel Zone Plate. Instead of focusing light using refraction, as is the case with a traditional lens, a zone plate focuses light using diffraction. This is accomplished by blocking light from passing through any areas that would create destructive interference at the focal point, while allowing light to pass through the zones that create constructive interference at the focal point. Figure 1.3 shows a simple example of a binary amplitude zone plate. In the same manner as with a linear diffraction phase grating, the efficiency of a zone plate can be improved by changing the phase of the light in the destructive zones by 180 degrees instead of blocking it. This was an idea that was originally suggested by British physicist Lord Rayleigh in 1871[5] but it was first demonstrated to have more than a six-fold improvement in the intensity of the focused light by Robert W Wood in 1898[6]. Although this thesis is not dealing with Fresnel zone plates specifically, the main topic of this thesis is the production of circular phase gratings similar to those conceived by Lord Rayleigh and produced by Wood.

Figure 1.3 – A Fresnel zone plate focuses light by using diffraction and is an example of a specialized circular diffraction grating. The example shown here can be classified as a binary amplitude zone plate where the black areas represent zones where light is completely blocked and the white areas represent areas where all of the light is allowed to pass through.[b]

1.3 Modern applications of diffraction gratings

Diffraction gratings have a wide range of applications. Because of their ability to disperse different frequencies of light, diffraction gratings can often be used as a replacement for prisms. One of their most common applications is in spectroscopy where a diffraction grating is used to separate the spectral components of a source of light. A spectrometer can work over a range of wavelengths from X-rays to infrared light using different diffraction gratings with optimized pitches and grating profiles. Analysis of the absorption and emission lines of the spectrum can tell a great deal about the source of light as well as what sort of materials the light passed through on the way to the detector. For these reasons, spectroscopy can provide a wealth of information in fields that use passive observations of light such as astronomy and remote sensing.

Diffraction gratings also change the direction of incoming light through diffraction orders higher than zero. With a carefully chosen combination of wavelength, grating pitch

[b] "Zone plate" by Tom Murphy VII - Based on GFDL/cc-by-sa Image:zone plate.png. Licensed under Creative Commons Attribution-Share Alike 3.0 via Wikimedia Commons - http://commons.wikimedia.org/wiki/File:Zone_plate.svg#mediaviewer/File:Zone_plate.svg

and incident angle, this can be used to couple and de-couple light in fibre optics or other optical waveguides. Prisms can also be used to couple light in this way; however diffraction gratings have the additional flexibility of being able to chirp the grating pitch. Because of the interdependence between wavelength and grating pitch, chirped gratings can be designed as grating band-pass filters or band reflectors so that a range of wavelengths are transmitted or reflected. One example is a fibre Bragg grating, which can be made from alternating materials with different indices of refraction within the core of a fibre optic. This type of diffraction grating is known as a volume phase grating since it is not the surface of the material, but the volume of the material, that alters the phase of light through variations of its index of refraction. The periodic changes in the index of refraction can be tuned to act as a dielectric mirror which maximizes reflection for certain wavelengths through constructive interference while limiting transmission through destructive interference. Chirping the pitch of this type of volume phase grating can serve to widen the band of the filter, and has useful applications in the field of communication such as in multiplexors in fibre optics[7].

Another interesting application for diffraction gratings is their use for the excitation of surface plasmons. When a thin layer of metal is interfaced with a dielectric material, under the right conditions it is possible to excite an electron density fluctuation in the surface of the metal by using light. This electron density wave is called a surface plasmon. One method of achieving this is by tuning the pitch of a diffraction grating on the surface of the metal to the specific plasmonic frequency of the interface. In this case, the diffraction grating changes the momentum of light towards the plane of the interface and allows surface plasmon resonance to take place in the metal film when the proper conditions are met. The resulting plasmon can then retransmit its energy as light at a specific frequency or band of frequencies, producing a tell-tale signal in its emitting spectrum. Surface plasmons are extremely sensitive to changes of the index of refraction at the interfaces and so can be used as biosensors in the direct detection of biomolecules as they associate or dissociate on the surface of the detector[8].

1.4 Photo-induced movement in azobenzene materials

Azobenzene is a chemical compound made of two phenyl rings attached by a nitrogen double bond. They can be considered as a derivative of diazene, a class of molecules which are strong absorbers of light and often used as dyes in industrial applications[9]. Azobenzene molecules exhibit an interesting property called photo-

isomerization. The molecule will change from its trans configuration to its cis isomer, and back again, when it is exposed to an absorbed frequency of light as illustrated in Figure 1.4. Azobenzene can be added as a chromophore to other materials such as polymers or glass forming materials and it will still retain its photo-isomerization properties. A fascinating result of the photo-isomerization of azobenzene in polymers is the photo-induced mass transport of the molecules. This was discovered in 1995 through the formation of Surface Relief Gratings (SRGs) in thin films of azopolymer by the Natansohn/Rochon[10] and Tripathy/Kumar[11] research teams. When an interference pattern of alternating dark and light fringes is projected with sufficient power and the correct wavelength onto a thin film of azobenzene functionalized material, the material will move away from the light towards the dark areas, effectively recording the interference pattern in surface-relief on the film. This method has proven to be an extremely simple single-step process to manufacture quality SRGs on a micro and nanometer scale. Although the physics behind the mass flow properties are not completely understood, one noteworthy feature that must be included in the development of theories of photo-induced transport in azo-materials is that it is dependent on the polarization of the incoming light. Experiments have shown that a combination of light intensity as well as variations in the electric field with a component along the grating vector direction is required to produce deep SRGs in azo-materials[12].

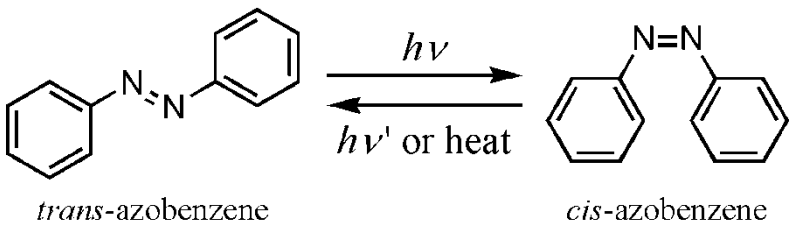

Figure 1.4 – In the proper conditions, azobenzene molecules change from one molecular isomer to another and back again when exposed to light in an effect called photo-isomerization.[c]

The synthesis of molecular glass has several advantages over polymers including higher yields and easier purification. Although they are not the first to synthesize azobenzene

[c] "Azobenzene isomerization". Licensed under Public domain via Wikimedia Commons - http://commons.wikimedia.org/wiki/File:Azobenzene_isomerization.png#mediaviewer/File:Azobenzene_isomerization.png

derivatives capable of forming glassy phases, a joint group from the Royal Military College of Canada and Queen's University has recently demonstrated a new azo-glass compound[13]. This material possesses the added benefits of a single step synthesis process. It has been shown that this azo-glass material is able to produce high quality photo-induced SRGs on a thin film with less than 50mW/cm^2 of irradiance from the inscribing source of light[13]. This azo-glass is the sample material that is used to create surface relief gratings in the experimentation section of this thesis.

1.5 Goal of Research

The goal of this thesis is to introduce a novel method of inscribing circular SRGs onto azo-glass films using a three-dimensional (3D) beam splitting technique with a fixture called a Circular Diffraction Grating Generator (CDG). The CDG's mirrored surface simultaneously acts to split and redirect a beam of coherent light to form interference fringes in the pattern of concentric circles. When a thin film of azo-glass material is placed at the small aperture of the CDG, the circular interference pattern is recorded in surface-relief on the film. This thesis will develop the theory required to relate the pitch of circular gratings generated to the geometry of the CDG when using a planar wave front as an inscribing source. In addition, this thesis will investigate the resulting pitches of circular SRGs produced by a CDG when the wave front of the light source is spherically divergent or convergent.

1.6 Thesis Structure

This thesis is divided into 6 chapters. Chapter 1 will serve as an introduction to some of the basic concepts and vocabulary required to understand the research. Following an introduction to diffraction gratings, including some necessary definitions, there is a short history on the early discoveries in the field of diffraction optics. Next, there is a short description of some modern applications of diffraction gratings. It concludes with a brief discussion detailing the goal of research and an outline of the thesis structure.

Chapter 2 is a literature review to determine current manufacturing techniques and possible applications for circular SRGs.

Chapter 3 will cover the derivation of the required theory. It will start with some basic concepts introducing light as an electromagnetic wave and the interference of light. It will review some theory on far-field diffraction as well as the derivation of the grating

equations. It will then provide a detailed geometric analysis of the interference patterns created by a CDG for both planar (collimated) as well as curved (divergent and convergent) sources of light. The last section in chapter 3 will go into some detail of the theory behind the critical height of the CDG and how it plays a role in the formation of circular or ring gratings.

Chapter 4 outlines the experimental procedures used to verify the theory. It will cover the details on how sample thin films of azo-glass material and the CDG fixtures themselves are produced. Next, it will explain the experimental set-up for producing circular SRGs with a collimated beam. Lastly, it will show the experimental set-up for producing circular SRGs with a curved wave front.

Chapter 5 will provide the results from the experiments outlined in Chapter 4 and will compare them with the theory from Chapter 3.

Chapter 6 will discuss the implications of the work and will summarize the conclusions of this thesis.

CHAPTER 2: LITERATURE REVIEW

2.1 Manufacturing techniques for diffraction gratings.

SRGs can be produced by a variety of methods. Gratings can be mechanically cut into a polished surface with a diamond tipped ruling engine. Early versions of this type of machine used very precise gearing mechanisms to control the spacing between each grating line. Modern ruling engines are now computer controlled and can employ piezoelectric actuators combined with high precision feedback control systems to further increase the accuracy of the grating profile to under 4 nm with the theoretical capability of inscribing gratings with pitches as small as 6000 lines per millimetre or a grating pitch of about 170 nm[14]. These types of ruling engines are one of the best manufacturing methods for creating master copies of large scale gratings. However, the ruling engines are very expensive pieces of equipment and can take days to inscribe a grating since each groove is cut one at a time. As an example, a 500 mm by 400 mm grating can take more than 720 hours of continuous operation of a ruling engine to create[14].

Other methods of direct grating patterning are the result of high precision computer aided nano-manufacturing techniques such as electron beam lithography[15], focused ion beams[16] or laser milling[17]. These methods can be time consuming for large grating areas since, similar to ruling engines, each line is milled individually making for relatively slow production speed. Depending on the power of the machine and the depth of grating required, the manufacturing time can be substantially slower than a ruling engine. For example, creating a grating with 1700 lines per millimetre (approximately 600nm pitch) on a 4 cm^2 area would take 6800 hours with a writing speed of 10 cm/hr as one paper reports[15]. Although these methods can be used to create very high quality gratings with nano-scale resolutions, they too require expensive specialized equipment.

Photolithography is widely used in the industry and involves using a photo-mask to expose a pattern onto a light sensitive material called a photo-resist. The photo-resist is chemically altered by the light, but only in the areas not blocked by the photo-mask. The surface can then be chemically treated to etch away or deposit material in the pattern that was photo-exposed onto the surface. The shapes and complexity of the pattern that can be created this way are limited only by the level of detail of the photo-mask and the resolution of the projection system. An alternative method of photolithography uses an interference

pattern from two or more coherent sources of light to directly expose the photo-resist without the use of a photo-mask. This method of fabrication is called interference photolithography and results in what's called a holographic grating. Holographic gratings are widely used in the field of optics and can be made with profile shapes that are approximately sinusoidal and have been shown to reduce optical aberrations that are normally present in ruled gratings[18]. Continued refinements in interference lithography methods have realized patterning resolutions of below 10 nm using extreme ultraviolet light wavelengths[19]. Photolithography is convenient for creating large and complex gratings quickly since the entire pattern is exposed simultaneously rather than written one line at a time. However, it is a complex multi-stage process which normally requires the production of the photo mask, exposure through a specialized projection system, chemical development of the photoresist, as well as etching and cleaning steps.

Nano-imprinting involves production of a mold, sometimes from a method listed above, which is then pressed into a polymer surface. Soft lithography is a type of nano-imprinting that uses a flexible mold to transfer a surface-relief pattern, such as a diffraction grating or Fresnel lens, onto a desired substrate[20]. The mold pattern can be modified prior to stamping through mechanical bending, compression or stretching[21] adding some additional versatility to this production method. Although nano-imprinting works well for mass production of gratings based on a master mold, it is also a multiple step process that is ill suited for rapid development of new prototype grating patterns.

A relatively new micro-fabrication technique called Direct Laser Interference Patterning utilizes two or more interfering beams of light to directly engrave microstructure surface patterns on commercially available polymers through laser ablation of the material[22]. Recent publications report grating pitches as small as 125 nm are possible using this technique[23]. This method has the benefits of traditional interference photolithography without the additional developing, etching and cleaning steps. However the ablation process used to form the material requires a high-powered pulsed laser.

2.2 Manufacturing of surface relief gratings in Azo-functionalized materials

Linear holographic SRGs fabricated using interference patterns projected onto azo-polymer films have been widely reproduced and studied since their discovery in 1995[10]. There are two main methods of manufacturing linear gratings in this method.

The first method involves splitting a laser beam with a beam splitter and then using mirrors to redirect the two beams in order to expose the sample of azo-material with laser light from at two different angles. The interference pattern of light caused by the angle between the beams can be inscribed directly on a film azo-material. This method is similar to the standard method of producing holographs and is therefore susceptible to vibration. Each optical element in the system must be extremely stable since any small movements, even at scales smaller than the wavelength of light, can affect the quality of the interference pattern by changing the phase position of the interfering light.

The second common method of fabricating linear SRGs in azo-films uses a Lloyd mirror as seen in Figure 2.1. A Lloyd mirror consists of a mirror that is held at a 90 degree angle to the sample. One half of the incident beam of light is reflected by the mirror while the other half strikes the sample directly. This creates an interference pattern of alternating light and dark fringes. The spacing of the fringes can be manipulated by rotating the entire fixture (sample and mirror) with respect to the angle of the incident beam. The main advantage to this method is that since the Lloyd mirror serves to split and redirect the incoming light in a single optical element, it is much less susceptible to vibration.

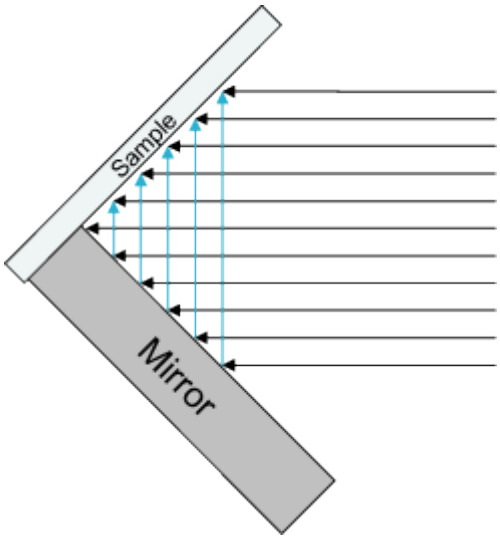

Figure 2.1 – Schematic of a Lloyd mirror set-up for inscribing linear SRGs in an azo-material sample. [d]

There is an excellent recent review article summarizing methods and applications of surface patterning on azo-polymers by Priimagi and Shevchenko[24]. The main advantage to producing diffraction gratings in this method is that it is a single step process that can produce large-scale gratings quickly without the requirement for a master photo-mask or mold. Grating spacing can be customized by changing the angle of the interfering beams or using different wavelengths of light[24]. However, a literature review on the subject has only turned up two other of publications reporting the fabrication of circular SRGs using azo-functionalized materials. These methods include the formation of circular diffraction gratings using Bessel beams[25] and fiber optic modes[26]. These techniques are somewhat similar in concept to the technique of using a CDG, in that they are using circular patterns of light to directly inscribe circular SRGs. However, the scale of the circular SRGs that have been produced by this method is in micrometers. The main advantage of the use of the CDG to generate circular gratings is the fact that it can create fairly large gratings on the order of 1 cm diameter in a single step process without a master grating pattern. It will be seen that the ability to make changes to the geometry of the CDG and the optical elements also adds an element of controllability to the size, grating pitch, and degree of chirp of the resulting circular SRG. This means that circular SRGs made to meet specific requirements can be quickly and easily fabricated using this new holographic method.

[d] Image from Brigham Young University website, http://www.photonics.byu.edu/holography.phtml

2.3 Applications for Circular Diffraction Gratings

As discussed in Section 1.3, linear diffraction gratings have a wide range of applications in modern technology. Circular diffraction gratings share similar properties as their linear counterparts, but because of their circular symmetry around an optical axis, they can be used in a variety of two-dimensional and on-axis applications. For example, circular diffraction gratings can be employed in the design of a wide variety of diffractive optical elements, such as diffractive or kinoform lenses[27], specialized diffractive lensacons[28] and hybrid lenses[29]. Optical sensors can sometimes benefit from the two-dimensional geometry of circular gratings to reduce the directional dependence of the gratings while enhancing sensitivity by using surface plasmons. This has been reported in applications such as infrared photodetectors[30] and plasmon enhanced biosensors[31]. An added benefit of the nano-manufacturing technology employed to make these gratings is that it can be used for the miniaturization of optical sensors and instruments. Micro-spectroscopes[32] and angular rotation sensors[33] have been shown to be technically feasible by using circular diffraction gratings with diameters less than 1mm across.

Another possible application for circular SRGs includes surface emitting distributed feedback lasers. A properly designed circular grating can act as a laser resonance cavity when pumped from an external optical source. This type of device has been reported as being produced by a variety of manufacturing techniques in chirped[34] and non-chirped configurations[35]. These tiny surface-emitting lasers can be manufactured at low costs and can be used as a coherent light source for a lab-on-a-chip or other miniaturized optical sensor applications.

An area of interesting research is the use of grating structures to create surface plasmon resonance to enhance the efficiency in light emitting diodes (LED) and solar cells. LED efficiencies and peak intensity outputs have been shown to increase through the use of a patterned metal surface capable of coupling surface plasmon modes[36]. The problem with extracting light is that the metal film attenuates its intensity through reflection and absorption. Grating structures have been shown to increase the photoluminosity intensity up to 46 times by increasing the light extraction efficiency and photon trapping in surface plasmon enhanced LEDs[37]. In a somewhat similar area of research, grating structures are being investigated as a tool to induce surface plasmons as well as couple waveguide modes into thin solar cell materials. In this case, the goal is to trap more light, instead of extracting

it as in the case with the LEDs. By incorporating repetitive circular nano structures into the fabrication of solar cells, it has been shown that an increase in the absorption of light by 7% is possible in thin film amorphous silicon solar cells[38]. Another paper reports a 43% increase in short circuit current for thin film silicon solar cells using a grating structure as compared to similar cells without these nano structures[39].

Another interesting application is the use of circular gratings as a photo-computation component. There is ongoing research to create a neural network architecture using two dimensional beam arrays of light. By interconnecting the beams of light in the beam array and by controlling the weight of these connections, it is possible to perform computations using light. One paper reports the use of binary Fresnel zone plates with a radius of 1.2 mm as diffractive optical elements for the generation of these beam arrays to create a photo-refractive neural network[40].

For all of the applications above, high quality circular diffraction gratings are required. It is possible that some of these types of research may be able to benefit from a way to produce holographic circular diffraction gratings.

CHAPTER 3: THEORY

3.1 Light as an electromagnetic wave

Light has been an object of great interest to humans since our earliest times. Astronomers and philosophers have been observing and trying to explain it for thousands of years. Under the scrutiny of some the greatest scientific minds, the past several centuries have yielded a tremendous advance in our understanding of the nature of light. We now know that light is a transverse wave that is able to propagate through certain materials and empty space through a series of alternating electric and magnetic fields. The accepted model that is currently used to describe the physics of an electromagnetic (EM) wave is the famous set of laws that make Maxwell's equations. An excellent summary of the theory of EM radiation can be found in the text book "Optics" by Hecht[41] and many of the formulas in this section were taken from chapter 3 of that book. Maxwell's equations can be used to describe the properties of the EM interactions in any material and are given as:

$$\oiint_A \vec{E} \cdot d\vec{S} = \frac{1}{\varepsilon_0} \iiint_V \rho dV \qquad (3.1.1)$$

$$\oiint_A \vec{B} \cdot d\vec{S} = 0 \qquad (3.1.2)$$

$$\oint_C \vec{E} \cdot d\vec{\ell} = -\iint_A \frac{\partial \vec{B}}{\partial t} \cdot d\vec{S} \qquad (3.1.3)$$

$$\oint_C \vec{B} \cdot d\vec{\ell} = \mu \iint_A \left(\vec{J} + \varepsilon \frac{\partial \vec{E}}{\partial t} \right) \cdot d\vec{S} \qquad (3.1.4)$$

$\vec{E}$ and $\vec{B}$ are the electric and magnetic vector fields. The electric permittivity ε and magnetic permeability μ are physical constants when in free space denoted by ε_0 and μ_0. The variable ρ is the charge density and $\vec{J}$ is the current density vector field. Equation (3.1.1) is known as Gauss's law for electric fields and describes how the total electric field flux over a closed area is related to the total amount of electric charge inside the volume of that same closed area. Equation (3.1.2) is called Gauss's Law for magnetic fields and is similar to equation (3.1.1) except since a magnetic monopole does not exist, it is impossible to have a point source or sink for a magnetic field. Therefore, the magnetic flux over a closed area will always be zero. Equation (3.1.3) is Faraday's Law which describes, more generally, how a time varying magnetic field can induce an electric field in a closed loop, thus generating electricity in a metal coil. Equation (3.1.4) is Ampere's Law and describes in

general terms how either a current or changing electric field can induce a magnetic field. Arguably, Maxwell's greatest contribution was recognizing that a flowing current was not necessarily required to create a magnetic field, but that any time varying electric field can induce a magnetic field. This realization allowed Maxwell to write his equations for free space, where there is no charge density or electric current density and where the permittivity and permeability are constants:

$$\oiint_A \vec{E} \cdot d\vec{S} = 0 \qquad (3.1.5)$$

$$\oiint_A \vec{B} \cdot d\vec{S} = 0 \qquad (3.1.6)$$

$$\oint_C \vec{E} \cdot d\vec{\ell} = -\iint_A \frac{\partial \vec{B}}{\partial t} \cdot d\vec{S} \qquad (3.1.7)$$

$$\oint_C \vec{B} \cdot d\vec{\ell} = \mu_0 \varepsilon_0 \iint_A \frac{\partial \vec{E}}{\partial t} \cdot d\vec{S} \qquad (3.1.8)$$

Remarkably, even though there are no electric charges, electrical currents, or any conductive materials in space, an EM wave can still form and propagate based on the interdependence of equations (3.1.7) and (3.1.8). It has been shown in appendix 1 of the text book by Hecht[41] that these two equations can be manipulated into their vector form:

$$\nabla^2 \vec{E} = \varepsilon_0 \mu_0 \frac{\partial^2 \vec{E}}{\partial t^2} \qquad (3.1.9)$$

$$\nabla^2 \vec{B} = \varepsilon_0 \mu_0 \frac{\partial^2 \vec{B}}{\partial t^2} \qquad (3.1.10)$$

These equations are well known forms of partial differential wave equations that describe a sinusoidal wave that propagates through time and space. According to wave theory the velocity of such a wave would be:

$$v = 1/\sqrt{\varepsilon_0 \mu_0} \qquad (3.1.11)$$

From Coulomb's law, which relates the force that is exerted between two charged particles, the value of the permittivity in free space can be determined experimentally as $\varepsilon_0 \approx 8.85 \times 10^{-12} s^2 C^2 m^{-3} kg^{-1}$. Because of the somewhat arbitrary selection of units for charge, time and distance, the permeability of free space is set as $\mu_0 = 4\pi \times 10^{-7} m \cdot kg \cdot C^{-2}$ to ensure the correct conversion between units of force and current from Ampere's force law, which relates the force acting on two wires with a certain current.

The result of $\varepsilon_0\mu_0 \approx 1.12\times10^{-18} s^2 m^{-2}$ can then be used with equation (3.1.11) to determine a velocity of approximately $3\times10^8 ms^{-1}$. This agrees very well with the measured speed of light in free space and offers convincing evidence that light is indeed comprised of electromagnetic waves.

It is sometimes convenient, knowing that both the electric and magnetic waves propagate together, to choose only one of these waves in order to simplify the expression of an EM wave. In practice, if the magnitude and direction of one is known at a given point in time and space, the same properties can be found for the other. One convention is to describe only the electric field $\vec{E}$ when working with light. This convention will be followed for the remainder of this thesis.

A complex number representation can be used to describe the amplitude of the electric field over time and space:

$$\vec{E}(\vec{r},t) = \mathrm{Re}\left[\vec{E}_0 e^{i(\vec{k}\cdot\vec{r}-\omega t+\varphi)}\right] \qquad (3.1.12)$$

or equivalently:

$$\vec{E}(\vec{r},t) = \vec{E}_0 \cos(\vec{k}\cdot\vec{r}-\omega t+\varphi) \qquad (3.1.13)$$

where $\vec{E}_0$ is the directional amplitude of the electric field, ω is the angular frequency $\omega = 2\pi\nu$ where ν is the frequency of light, and t is time. Additionally, $\vec{k}$ is the wave vector in the direction the wave is travelling and whose magnitude is $\left|\vec{k}\right| = 2\pi/\lambda$. Also, λ is the wavelength of light, and $\vec{r}$ is the position vector. Lastly, φ describes the phase position of the wave in radians.

The next simplification that will be made to our theory describing the propagation of electromagnetic waves is removing the time dependence. Imagine taking a snap shot of a waves moving in a swimming pool. The wave can still be described in terms of values for k and r, however by making t a constant at some arbitrary point in time, the term ωt becomes a constant. The constants ωt can be combined into the phase constant φ to describe phase position in space at that frozen point in time. The same concept can be applied to an electromagnetic field giving the result:

$$\vec{E}(\vec{r}) = \vec{E}_0 \cos(\vec{k}\cdot\vec{r}+\varphi) \qquad (3.1.14)$$

Since the light beams that will be used in our experiment come from a single coherent source, meaning the phase of the light will not change as it travels, the assumption can be made that the interference pattern from the time independent waves will also not depend on the intial phase variable φ from the source. This assumption is possible because any initial phase value at the source of light will cancel out when calculating the phase difference between the two beams where they meet at their interference point. The phase difference between the beams is calculated by subtracting path lengths $\vec{r}_1$ and $\vec{r}_2$, thereby eliminating the initial phase term from the common source. The result is the analysis of the interference of electromagnetic waves has been greatly simplified such that the only factors that need be considered are the path length $\vec{r}$ that the light beam travels and the wavelength of light from the equation $\left|\vec{k}\right| = 2\pi / \lambda$. Using the path length and wavelength of light rays to calculate the phase difference for interfering light is the basis for the geometric ray trace analysis that will be used in sections 3.5 and 3.6

3.2 Interference of light

Like most other forms of waves, EM waves follow the principle of superposition. This principle states that when two or more waves occupy the same location at the same time, the resulting wave will be equal to the sum of all the waves. Figure 3.1 represents two waves interfering with each other and the resultant superposition wave in red. For areas where the amplitudes of the interfering waves are both on the same side of the x axis, they will interfere constructively and the resulting superposition wave will be amplified. For areas where the amplitudes of the interfering waves are on opposite sides of the x axis, they will form destructive interference and they will partially or completely cancel each other out, reducing the amplitude of the resulting superposition wave. This principle of superposition is a very important concept since it explains many phenomena relating to light including diffraction.

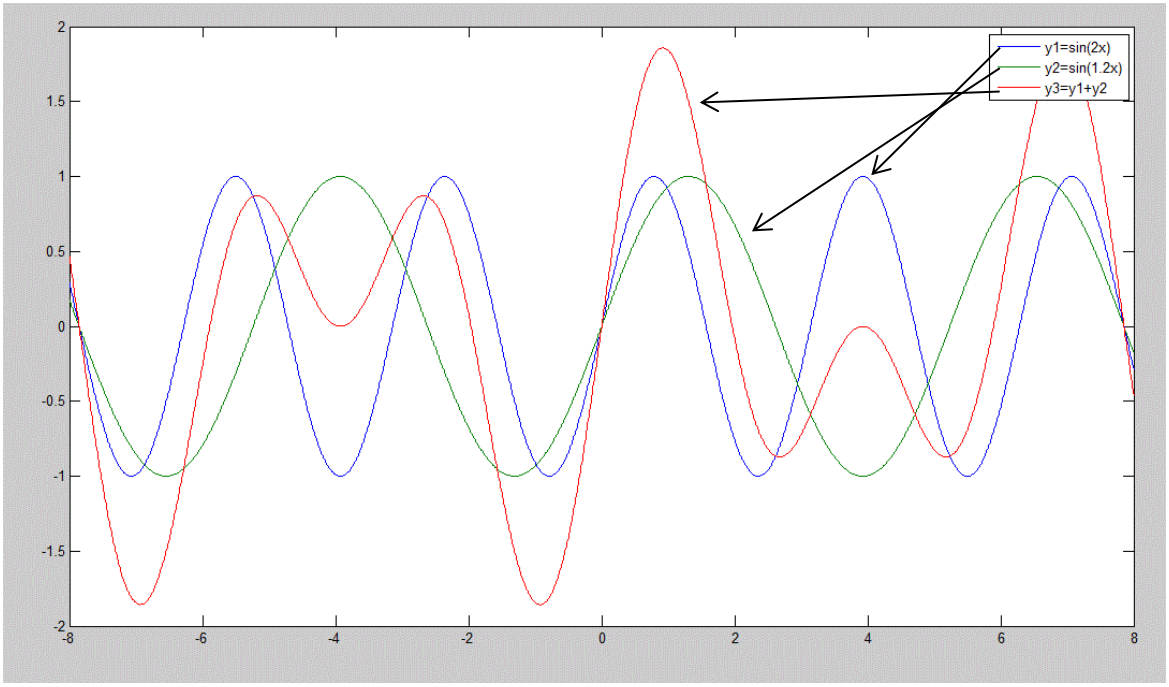

Figure 3.1 – A graph representing the superposition of waves. Two waves with different frequencies and an amplitude of 1 (arbitrary units) travel along the x axis. The resultant superposition wave is also shown.

3.3 Diffraction of light

According to the Huygens-Fresnel principle, any disturbance to a beam of light can be mathematically described as an infinite number of point sources along the wave front of the beam. The superposition of the waves emitted from all of these point sources is an effective way to model the bending and interference effects of light that occur at the edges of an interface, known as diffraction. Figure 3.2 shows a plane wave striking a slit. The wave front can be approximated as a number of point sources represented by the yellow dots. It can be seen that resulting wave front from the superposition of the point sources will continue on the same path in the middle of the slit, but will curve outward at the edges of the slit. An additional implication of this model, that is perhaps less obvious in Figure 3.2, is that a fringe pattern of alternating maxima and minima is created from the interference of the multiple point sources. Both the bending of light around the edges of an interface and the resulting interference pattern are exactly what is observed in nature as diffraction.

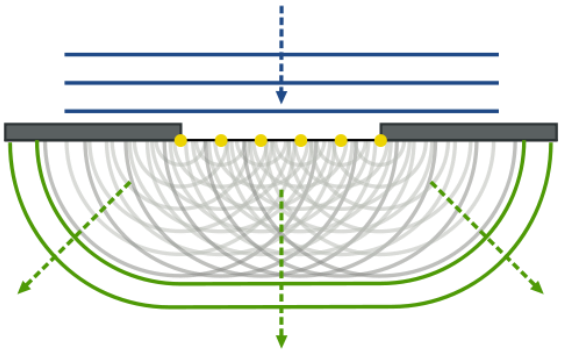

Figure 3.2 – Diffraction of a wave through a slit. The dots represent the conceptual point sources of light used by the Huygens-Fresnel principle[e]

A simple example of diffraction in everyday life can be seen in the shadow cast by an object. Any object blocking light can act as an interface and becomes a source of diffraction. Because the angle of diffraction is dependent on wavelength (this will be shown in the section 3.4), it is most noticeable when it comes from a coherent source, or a source that emits a single frequency of light. It is not easy to see diffraction patterns at the edges of the shadow of your hand in daylight because the different colours that make up white light all diffract at different angles making a clear pattern hard to discern. However, with a bright and coherent light source, it is possible to see interference patterns of alternating light and dark fringes at the edges of any shadow as a result of diffraction. An example of this phenomenon can be seen around the edges of a razor blade in Figure 3.3.

[e] By Arne Nordmann (norro) - Licensed under Public domain via Wikimedia Commons - http://commons.wikimedia.org/wiki/File%3ARefraction_on_an_aperture_-_Huygens-Fresnel_principle.svg

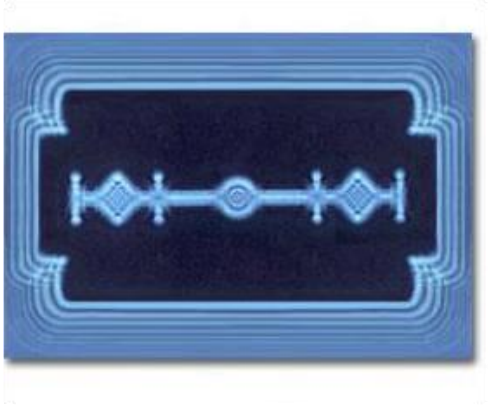

Figure 3.3 – The interference pattern in the shadow of this razor blade is caused by diffraction at the edges of the blade[f].

3.4 Diffraction gratings and the grating equation

As mentioned in section 1.1, a diffraction grating is a periodic modulation in a material that affects the properties of light. In order to better understand how a diffraction grating works, it is best to start with the simplest example, a transmission amplitude grating. In this example, we will assume that an array of thin slits with a space between them of d will act as an array of point sources as depicted in Figure 3.4.

[f] Image from Scientific America Blog: "X-Ray Crystallography: 100 Years at the Intersection of Physics, Chemistry, and Biology", http://blogs.scientificamerican.com/scicurious-brain/files/2012/12/diffraction-razor-blade.png.

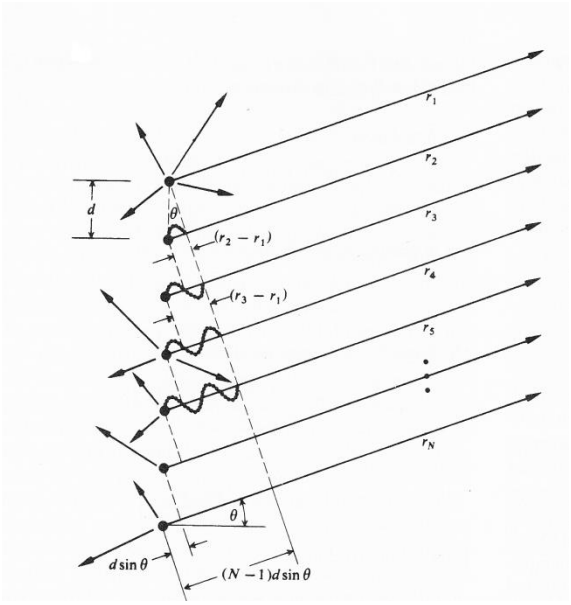

Figure 3.4 – Schematic of the geometry used to theoretically describe the far-field interference pattern from an array of coherent point sources.[g]

If the grating is illuminated (from the left of the diagram) with a normally incident collimated beam (that is to say a beam with a perfectly planar wave front), then the point sources will be emitting light that is perfectly in phase. If the collimated beam has an even power distribution over its entire wave front, then each point source will each emit an electric field that is equal and that will have an amplitude approximately equal to the value E_0 when it arrives at point P. Each point source, starting from the top of the diagram, is numbered with an integer n = 1, 2, 3, … , N where N is the total number of point sources in the array. The value r_n is the distance from each respective emitter to a distant point P. The resulting electric field amplitude, E, at point P will be equal to the total contribution of these emitters using equation (3.1.12) and can be written as:

$$E = E_0 e^{i(kr_1 - \omega t)} + E_0 e^{i(kr_2 - \omega t)} + \ldots + E_0 e^{i(kr_N - \omega t)} \qquad (3.3.1)$$

By taking out a common factor it can be further manipulated to show:

$$E = E_0 e^{-i\omega t} e^{ikr_1} \times \left[1 + e^{ik(r_2 - r_1)} + e^{ik(r_3 - r_1)} + \ldots + e^{ik(r_N - r_1)}\right] \qquad (3.3.2)$$

[g] Image from pg 450 of Hecht[41]

The slits initially all have the same phase, but because the path lengths r_n are all different this will introduce a phase difference between the rays arriving at point P. This phase difference ϕ can be defined in terms of the difference in distance between two rays multiplied by k:

$$\phi = k(r_2 - r_1) \tag{3.3.3}$$

From Figure 3.4, we see from similar triangles that the phase difference between two rays can be written more generally as $(n-1)\phi = k(r_n - r_1)$. Substituting this equation into equation (3.3.2) gives:

$$E = E_0 e^{-i\omega t} e^{ikr_1} \times \left[1 + e^{i\phi} + (e^{i\phi})^2 + ... + (e^{i\phi})^{N-1}\right] \tag{3.3.4}$$

The geometric series in the square brackets in equation (3.3.4) is known to equal:

$$\left[1 + e^{i\phi} + (e^{i\phi})^2 + ... + (e^{i\phi})^{N-1}\right] = \left(e^{i\phi N} - 1\right) / \left(e^{i\phi} - 1\right) \tag{3.3.5}$$

Taking out a common factor of $e^{iN\phi/2} / e^{i\phi/2}$ gives:

$$\left[1 + e^{i\phi} + (e^{i\phi})^2 + ... + (e^{i\phi})^{N-1}\right] = \frac{e^{iN\phi/2}\left[e^{iN\phi/2} - e^{-iN\phi/2}\right]}{e^{i\phi/2}\left[e^{i\phi/2} - e^{-i\phi/2}\right]} \tag{3.3.6}$$

Using the trigonometric identity $\sin a = \left(e^{ia} - e^{-ia}\right) / 2i$ and simplifying further gives:

$$\left[1 + e^{i\phi} + (e^{i\phi})^2 + ... + (e^{i\phi})^{N-1}\right] = e^{i(N-1)\phi/2}\left(\frac{\sin N\phi/2}{\sin \phi/2}\right) \tag{3.3.7}$$

Substituting equation (3.3.7) into equation (3.3.4) gives:

$$E = E_0 e^{-i\omega t} e^{i[kr_1 + (N-1)\phi/2]}\left(\frac{\sin N\phi/2}{\sin \phi/2}\right) \tag{3.3.8}$$

By changing the geometry of the problem by defining R as the distance from the centre of the array to the point P in question we see that:

$$R = \frac{1}{2}(N-1)(r_2 - r_1) + r_1 \tag{3.3.9}$$

By substituting equation (3.3.3) into equation (3.3.9) we get:

$$R = \frac{1}{2}(N-1)\frac{\phi}{k} + r_1 \tag{3.3.10}$$

And by rearranging we get:

$$kR = \frac{1}{2}(N-1)\phi + kr_1 \tag{3.3.11}$$

Subtituting this equation into equation (3.3.8) gives:

$$E = E_0 e^{i(kR-\omega t)}\left(\frac{\sin N\phi/2}{\sin \phi/2}\right) \qquad (3.3.12)$$

Irradiance is the measurement of the average energy over an area over a unit of time. It can be defined as a relation to the electric field in an EM wave by the expression:

$$I \propto \frac{E^* \cdot E}{2} \qquad (3.3.13)$$

where E* is the complex conjugate of the value E.

By using equation (3.3.13) with equation (3.3.12) and combining all of the constant variables into a single constant I_0 we get:

$$I = I_0 \frac{\sin^2(N\phi/2)}{\sin^2(\phi/2)} \qquad (3.3.14)$$

where I_0 is the irradiance from a single point source at point P. From Figure 3.4, we can see that the phase difference between any two consecutive emitters can be expressed as k times the difference in distance between two rays. This can be expressed in terms of the angle θ as:

$$\phi = kd\sin\theta \qquad (3.3.15)$$

Substituting equation (3.3.15) into equation (3.3.14) gives our final result of irradiance as a function of angle θ:

$$I = I_0 \frac{\sin^2\left(\frac{Nkd}{2}\sin\theta\right)}{\sin^2\left(\frac{kd}{2}\sin\theta\right)} \qquad (3.3.16)$$

This equation tells us that if N is larger than 1, then the top half of the expression will modulate between light and dark fringes more often than the bottom half of the expression. Figure 3.5 is an example graph of equation (3.3.16) for N=10. The three tall peeks represent the diffraction orders 0, 1, and -1 and are the result of the slower modulation from the bottom portion of the equation. The faster modulated smaller peeks are a result from the top half of the equation. For larger values of N, the number and frequency of these peeks becomes so large that they are nearly impossible to resolve spatially and so the principal diffraction order maxima remain the primary features of the diffraction pattern.

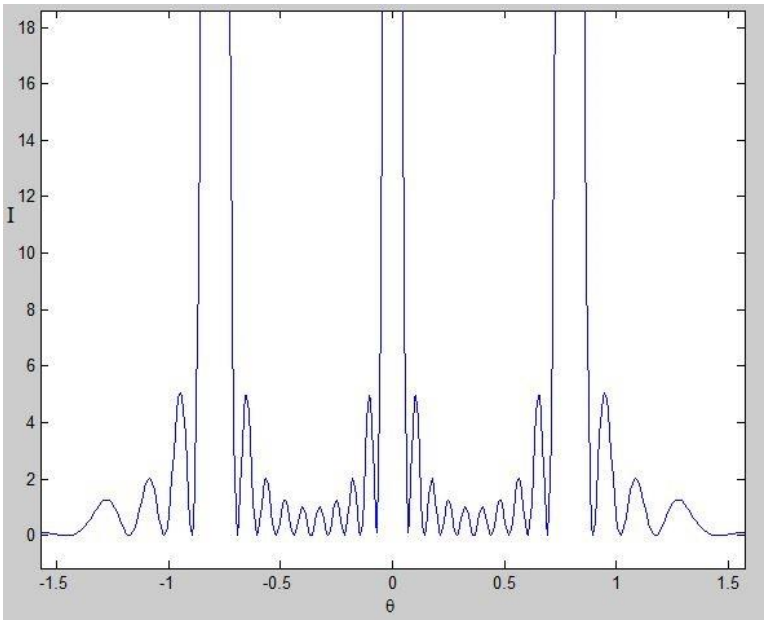

Figure 3.5 – Graph of irradiance versus diffraction angle from equation (3.3.16) with N=10, I_0=1 Wm^{-2}, λ=532nm and d=750nm.

In order to find the principal maxima we must set the bottom half of the expression from equation (3.3.16) to zero.

$$0 = \sin^2\left(\frac{kd}{2}\sin\theta\right) \qquad (3.3.17)$$

Therefore the value inside the brackets of equation (3.3.17) must be equal to:

$$\pi m = \frac{kd}{2}\sin\theta$$

$$2\pi m = kd\sin\theta_m \qquad (3.3.18)$$

where $m = 0, \pm 1, \pm 2, \ldots$ serves as an integer multiplier, and indicates the order of the diffraction maximum as previously defined.

This result makes intuitive sense since going back to equation (3.3.15), we know that the phase difference ϕ between two consecutive rays at a certain angle θ_m must be some multiple of 2π for fully constructive interference to occur. From the similar triangles in Figure 3.4, we know that all of the emitters will have fully constructive interference at this angle because their phase differences will likewise be multiples of 2π.

The final result, by substituting the definition of $k = 2\pi / \lambda$ into equation (3.3.18), is:

$$m\lambda = d\sin\theta_m \qquad (3.3.19)$$

This equation is known as the grating equation for normal incidence. An approximation was cleverly included into Figure 3.4 such that all of the rays r_1 to r_N are approximately parallel to each other. This occurs when the distance from the grating to the screen, r, is much larger than the distance d between point sources. This is known as the far field or Fraunhofer approximation.

As its name implies, the grating equation for normal incidence only applies when the incident light is normal to the grating. If the angle of incidence were to change, the point source emitters in Figure 3.4 would no longer emit perfectly in phase because of the different path lengths from the source. This would be equivalent to adding some new phase shift ψ between each consecutive emitter. From equation (3.3.15) this gives:

$$\phi = kd\sin\theta \pm \psi \qquad (3.3.20)$$

The plus or minus sign signifies that phase shift could be added or subtracted depending on which quadrant the angle of incidence is in. The value of ψ from the off-normal incident light can be easily described by using Figure 3.4 with the direction of light reversed. In this case:

$$\psi = kd\sin\theta_i \qquad (3.3.21)$$

where θ_i is the angle of incidence. Substituting equation (3.3.21) into equation (3.3.20) and solving to find the principle maxima of equation (3.3.14) similar to what was done for the case of normal incidence yields the result:

$$d\sin\theta_m = m\lambda \pm d\sin\theta_i$$

$$d(\sin\theta_m \pm \sin\theta_i) = m\lambda \qquad (3.3.22)$$

This is a more general solution to the grating equation that works for any angle of incidence.

Although our grating equations were derived using an array of point source emitters, it can be similarly derived and applied to many different types of diffraction gratings under the same far field approximation. In the case for gratings that are not an array of point sources the periodic distance between emitters d, is equivalent to the grating pitch Λ.

As mentioned in the introduction section, one advantage of a phase grating over an amplitude grating is that none of the incident light is blocked in a phase grating. This results in a large increase in the grating's diffraction efficiency. The derivation of the grating equation for a sinusoidal phase grating is more complicated than the simple example shown here. However, for a square wave phase grating, it is relatively easy to conceptualize that by

changing the phase of light by 180 degrees in zones where destructive interference would normally occur (areas that would be blocked by a amplitude grating), you would actually be creating additional zones of constructive interference. Therefore, the square wave phase grating is equivalent to doubling the number of constructive source emitters compared to a similar amplitude grating. Because irradiance is related to the electric field times its complex conjugate the result effectively quadruples the irradiance of a square phase grating compared to a binary amplitude grating. This example illustrates why phase gratings are so much more efficient than their amplitude grating counterparts.

3.5 Analysis of the fabrication of constant pitch circular gratings using a planar wave front

Assume a mirror in the shape of a hollow truncated cone. The inner surface of this shape is reflective and is the basis for a theoretical CDG. When a collimated laser beam with a diameter sufficiently large to illuminate the entire reflective surface is incident perpendicular to the sample, the CDG will reflect the light towards the smaller aperture end, creating an interference pattern where it interferes with the directly incident light. Figure 3.6 shows a schematic of the cross section of a planar wave front incident onto a CDG where θ is the angle between the mirrored surface and the normal.

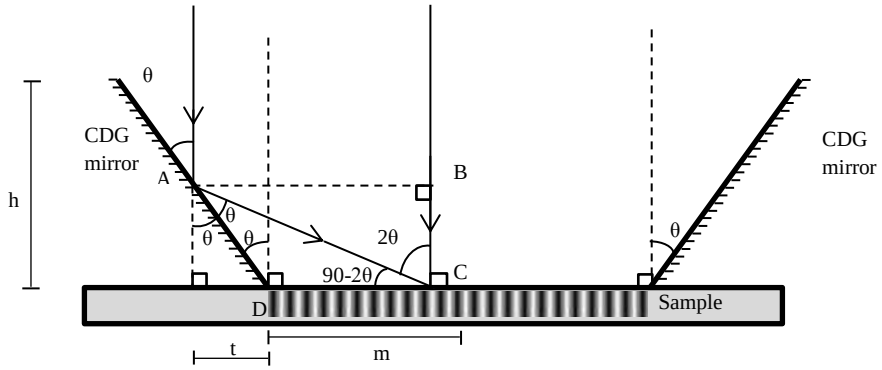

Figure 3.6 – Schematic showing the geometry of a CDG with a mirror angle θ when it is exposed to a planar wave front

At points A and B, the collimated wave front will be in phase. Using the law of sines with triangle ACD, it can be seen that:

$$\frac{\sin(90+\theta)}{AC} = \frac{\sin(\theta)}{DC}$$

Giving:

$$AC = DC\cot\theta \qquad (3.4.1)$$

Using triangle ABC, it can be shown that:

$$BC = AC\cos 2\theta \qquad (3.4.2)$$

Substituting equations (3.4.1) and (3.4.2) to find the difference in path length PD is:

$$PD = AC - BC = DC\cot\theta - AC\cos 2\theta \qquad (3.4.3)$$

Substituting equation (3.4.1), into equation (3.4.3) gives:

$$PD = AC - BC = DC\cot\theta - DC\cot\theta\cos 2\theta$$

$$PD = AC - BC = DC\cot\theta(1-\cos 2\theta) \qquad (3.4.4)$$

And from the trigonometric identity, $\cos 2\theta = 1 - 2\sin^2\theta$ we get:

$$PD = AC - BC = DC\cot\theta(1-[1-2\sin^2\theta])$$

$$PD = AC - BC = \frac{DC2\sin^2\theta}{\tan\theta}$$

$$PD = AC - BC = DC2\sin\theta\cos\theta \qquad (3.4.5)$$

From the trigonometric identity $\sin 2\theta = 2\sin\theta\cos\theta$ we get:

$$PD = AC - BC = DC \sin 2\theta \qquad (3.4.6)$$

The phase difference ϕ between the two paths is related to the path length difference by the expression:

$$\phi = k(PD + \Delta) \qquad (3.4.7)$$

where k is the wavenumber for the light source $k = 2\pi / \lambda$, and the additional term of Δ is the phase change on path AC from a single reflection on the CDG mirror. In order to find the grating pitch Λ or the distance between each maxima, we need to find the distance between two separate, but very close points on the sample where the change in the phase difference $\Delta\phi$ between interfering paths will be 2π. This can be written as:

$$\Delta\phi = \phi_2 - \phi_1 = 2\pi \qquad (3.4.8)$$

Substituting equation (3.4.7) into equation (3.4.8) gives:

$$\Delta\phi = 2\pi = k\left[\left(PD_2 + \Delta\right) - \left(PD_1 + \Delta\right)\right] \qquad (3.4.9)$$

By substituting the definition of k and equation (3.4.6) into (3.4.9) we get:

$$2\pi = \frac{2\pi}{\lambda}(DC_2 \sin 2\theta - DC_1 \sin 2\theta) \qquad (3.4.10)$$

Since we know the distance between DC_2 and DC_1 will be equal to the pitch of the grating given the condition from equation (3.4.10) is met, therefore we can write:

$$\Lambda = DC_2 - DC_1 = \lambda \csc 2\theta \qquad (3.4.11)$$

This equation is our final result and relates the pitch of the circular grating generated to the angle of the CDG θ, and wavelength of light λ, when using a collimated source. It also demonstrates a practical limit to the smallest grating pitch that can be generated which is dependent on the wavelength of the light source and is limited to $\Lambda \approx \lambda$ as θ approaches 45 degrees. At CDG angles greater or equal than 45 degrees, the reflected light will never reach the sample surface and no interference pattern will be generated.

3.6 Analysis of the fabrication of chirped pitch circular gratings using curved wave fronts

Taking the same theoretical conical CDG mirror as in the last section, we now investigate the result of a point source of coherent light placed at a distance s from the center of the fixture along the axis of symmetry. The CDG will again reflect the light towards the smaller aperture end, creating an interference pattern with the directly incident light, but because of the curvature of the wave front, the mathematics becomes more complicated.

Figure 3.7 shows a schematic of the point source located at point A and its corresponding reflected image source at point I due to the CDG mirror.

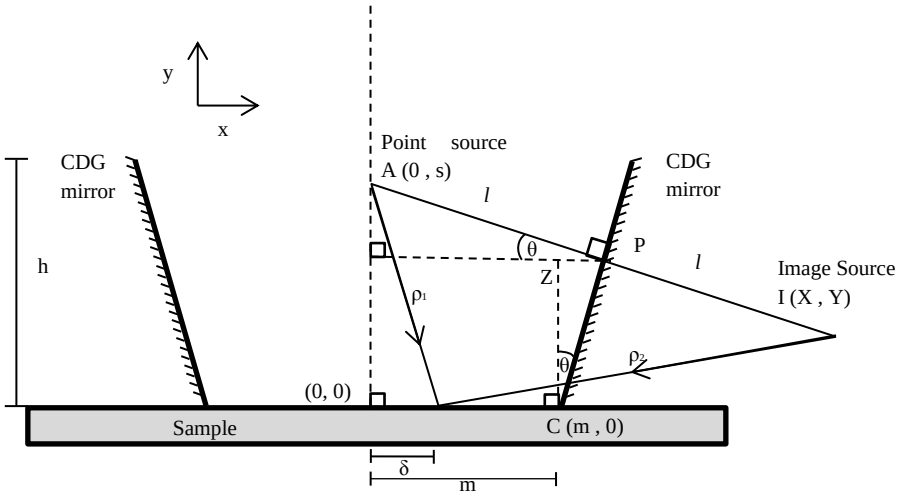

Figure 3.7 – Schematic for the geometry of a divergent point source used with a CDG to create chirped circular gratings

Using Cartesian co-ordinates, from diagram the Point P is located at:

$$(l\cos\theta, s - l\sin\theta) \qquad (3.5.1)$$

Because the Image Source at point I will be twice the distance from A as the point P:

$$(X,Y) = (2l\cos\theta, s - 2l\sin\theta) \qquad (3.5.2)$$

In order to find the distance *l*, from triangle CZP we take:

$$\tan\theta = \frac{l\cos\theta - m}{s - l\sin\theta}$$

which can be further manipulated to show that:

$$l = s\sin\theta + m\cos\theta \qquad (3.5.3)$$

Substituting this value of *l* into (3.5.2) and reducing (using common double angle and half angle trigonometric identities) gives:

$$(X,Y) = (2(s\sin\theta + m\cos\theta)\cos\theta, s - 2(s\sin\theta + m\cos\theta)\sin\theta)$$

$$(X,Y) = (2s\sin\theta\cos\theta + 2m\cos^2\theta, s - 2s\sin^2\theta + 2m\cos\theta\sin\theta)$$

$$(X,Y) = (m\cos(2\theta) + m + s\sin(2\theta), s\cos(2\theta) - m\sin(2\theta)) \qquad (3.5.4)$$

Now that we have the locations of point A and point I in terms of the parameters θ, m, and s, we can use their locations to calculate the difference in their effective optical path lengths to a given point (0, δ). Again we define the path length difference as $PD = \rho_2 - \rho_1$.

Given from Figure 3.7 that,

$$\rho_1 = \sqrt{\delta^2 + s^2} \tag{3.5.5}$$

$$\rho_2 = \sqrt{(X - \delta)^2 + Y^2} \tag{3.5.6}$$

We can expand our definition of PD and substitute in equation (3.5.4) to get:

$$PD = \sqrt{2sm\sin(2\theta) - 2s\delta\sin(2\theta) + s^2 + 2m^2\cos(2\theta) + 2m^2 - 2m\delta\cos(2\theta) - 2m\delta + \delta^2} - \sqrt{\delta^2 + s^2} \tag{3.5.7}$$

Similar to the last section, the phase difference between the two paths is related to the path length difference and is given by:

$$\phi = k(PD + \Delta) = \frac{2\pi}{\lambda}(PD + \Delta) \tag{3.5.8}$$

Again, the extra term Δ is the phase shift due to the single reflection which takes place on the ρ_2 optical path. In the same manner as before, if we set the change in phase difference $\Delta\phi$ between two different points δ_1 and δ_2 to be equal to 2π, this gives us:

$$\Delta\phi = 2\pi = \frac{2\pi}{\lambda}\left[\left(PD_2(\delta_2) + \Delta\right) - \left(PD_1(\delta_1) + \Delta\right)\right]$$

$$1 = \frac{1}{\lambda}\left[PD_2(\delta_2) - PD_1(\delta_1)\right] \tag{3.5.9}$$

Here we are using function notation for the path length difference PD to show its dependence on the parameter δ as seen in equation (3.5.7). The other variables that the path difference depends on: m, s, and θ are effectively constants for a given geometry of a specific experimental set-up. In order to simplify the analysis, they will be treated as such.

An analysis of Figure 3.8 for a light source converging onto a virtual point A yields similar results as for the divergent case.

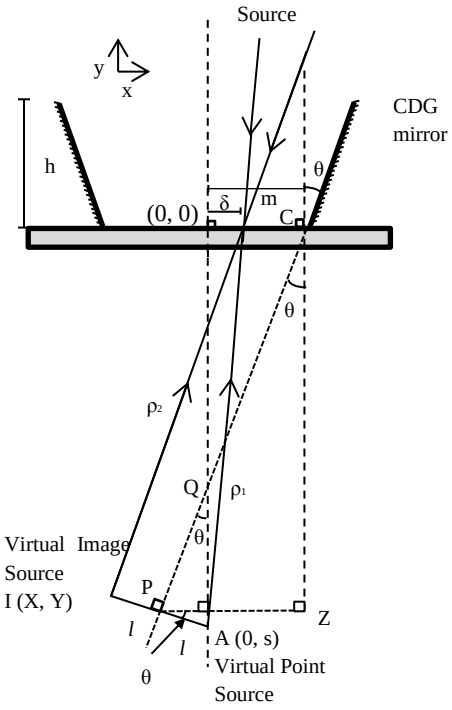

Figure 3.8 - Schematic for the geometry of a convergent source to a virtual point A using a CDG to create chirped circular gratings

Here the value of s will be negative and point P will have the co-ordinates:

$$(-l\cos\theta, s + l\sin\theta) \tag{3.5.10}$$

From triangle CZP, still maintaining the s has a negative value, we know that:

$$\tan\theta = \frac{(m + l\cos\theta)}{-(s + l\sin\theta)} \tag{3.5.11}$$

which further reduces to:

$$l = -m\cos\theta - s\sin\theta \tag{3.5.12}$$

From Figure 3.8 knowing that the location of the image source is:

$$I(X,Y) = (-2l\cos\theta, s + 2l\sin\theta) \tag{3.5.13}$$

Substituting in equation (3.5.12) into (3.5.13) yields:

$$(X,Y) = (2(s\sin\theta + m\cos\theta)\cos\theta, s - 2(s\sin\theta + m\cos\theta)\sin\theta) \tag{3.5.14}$$

This equation (3.5.14) is precisely equivalent to equation (3.5.4) derived from the diverging source case above. This equivalency holds true so long as the virtual point source A is lower than point Q (0, -m/tanθ) where mirror line intersects the axis of symmetry or mathematically:

$$s < -m / \tan\theta \qquad (3.5.15)$$

If the location of the virtual point source was above point Q on the diagram, then the angle of the converging light would be steeper than the CDG angle. In this case the CDG mirror would fall into its own shadow and no light would hit the mirror at all.

Unlike the last section where we analysed a collimated source beam to inscribe constant pitch SRGs, in the chirped pitch configuration it is impossible to isolate the parameter δ from equation (3.5.9) to get a spatial representation of the grating pitch $\delta_2 - \delta_1$ through algebraic manipulation. In order to overcome this problem, a computer simulation using a ray trace analysis method was developed in order to measure the distance beams of light travel before meeting at a position (δ, 0) on the sample. By taking multiple virtual test paths for the rays of light, the simulation can provide an estimate of the grating pitch as a function of δ which can be graphed for a given experimental geometry. This computer simulation was independently verified by using commercial algebra software to numerically solve equation (3.5.9) with equation (3.5.7) for certain test cases with the same set geometry as the simulation. The results of this simulation will be presented in the section 4.5. The MATLAB source code for the ray trace simulation is found at Appendix A:

3.7 Critical height of the CDG

The ratio of the height of the CDG fixture h, to the radius of the minor aperture, m, is a critical parameter that also depends on the CDG angle. If the height of the CDG is too great, then the reflected beam will cross the centre mark of the circular SRG being inscribed and create additional unwanted interference with the beams from the opposite side of the CDG. If the height of the CDG is too small, then the reflected beam will not reach the centre point of the circular SRG at all and the result will be a ring grating instead of a full circular grating.

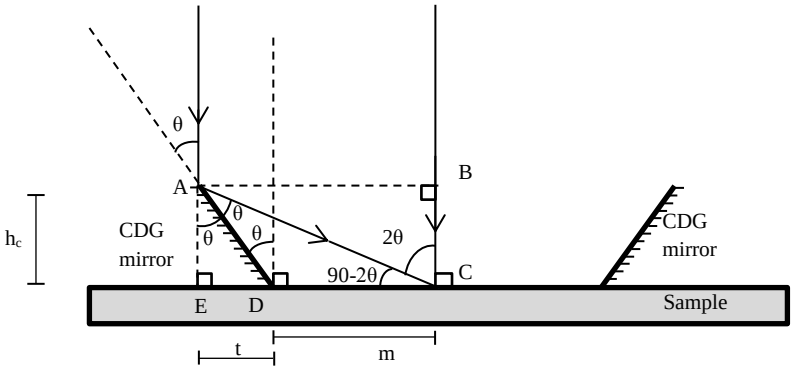

Figure 3.9 – Geometry to calculate the critical height of the CDG with collimated beam

The critical height of the CDG, h_c, is defined as the height which causes the reflected beam to strike the centre of the circular grating. Using triangle ADE from Figure 3.9 it can be shown that:

$$h_c = \frac{t}{\tan\theta} \tag{3.6.1}$$

Using triangle ABC it can be shown that:

$$\frac{m+t}{h_c} = \tan 2\theta \tag{3.6.2}$$

Isolating for t from equation (3.6.2) gives:

$$t = h_c \tan 2\theta - m \tag{3.6.3}$$

Substituting equation (3.6.3) into equation (3.6.1) it can be shown that:

$$h_c = \frac{m}{\tan 2\theta - \tan\theta} \tag{3.6.4}$$

This expression defines the critical height of the CDG for inscribing constant pitch SRGs with a collimated wave front in terms of the two other CDG parameters m and θ.

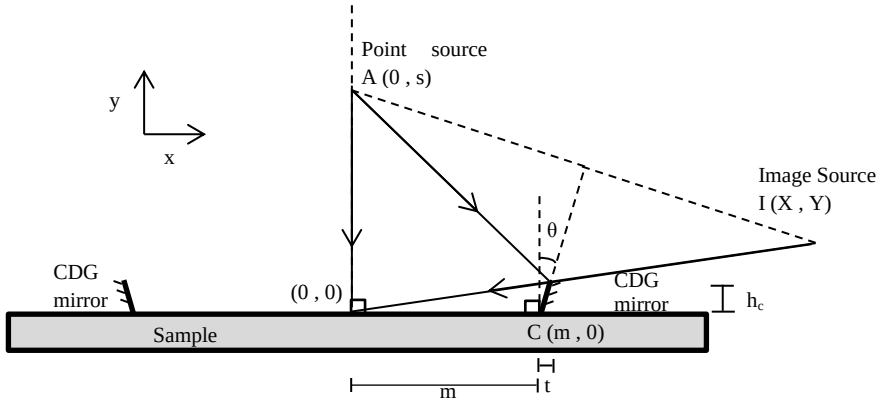

Figure 3.10 - Geometry to calculate the critical height of the CDG with divergent beam

In the case of a convergent or divergent wave fronts used for inscribing chirped pitch SRGs, the calculations are complicated by the additional parameter s. Figure 3.10 shows the geometry for calculating the critical height of the CDG for a divergent beam. From equation (3.5.4) we know the position of I is equal to:

$$(X,Y) = (m\cos(2\theta) + m + s\sin(2\theta), s\cos(2\theta) - m\sin(2\theta)) \qquad (3.6.5)$$

We can use the standard equation for a line to describe a line from point I to the origin as:

$$y = \frac{Y}{X}x = \frac{s\cos 2\theta - m\sin 2\theta}{m\cos 2\theta + m + s\sin 2\theta}x \qquad (3.6.6)$$

We can also describe the line that coincides with the CDG mirror as:

$$x = y\tan\theta + m \qquad (3.6.7)$$

To find the point of intersection of these two lines, we substitute equation (3.6.7) into equation (3.6.6) and simplify with trigonometric identities to get:

$$h_c = y = \frac{m\left(s\cos 2\theta - m\sin 2\theta\right)}{2m + s\tan\theta} \qquad (3.6.8)$$

This equation represents the critical height of a CDG when inscribing with a divergent wave front. Since we know that Cartesian co-ordinate location equations from the Image Source I are equivalent for converging and diverging beams from equations (3.5.4) and (3.5.14), we know that equation (3.6.8) will also hold true for the case of a converging light source (s<0).

However, applying the constraint that the critical height must be a positive value allows us to gain more insight into the geometry of a converging or diverging beam used with a CDG using equation (3.6.8). If s is greater than zero, as with a diverging beam, then the value in brackets of equation (3.6.8) must also be greater than zero in order to get a positive critical height giving:

$$s\cos 2\theta > m\sin 2\theta$$

$$s > m\tan 2\theta \qquad (3.6.9)$$

If value of s is smaller than the value given by equation (3.6.9), then the bottom half of equation (3.6.8) must be negative to give a positive value to h_c. This means that:

$$0 > 2m + s\tan\theta$$

$$s < \frac{-2m}{\tan\theta} \qquad (3.6.10)$$

Equations (3.6.9) and (3.6.10) constrain the possible values of s for a given CDG geometry if a full circular grating is desired with no cross over interference. From the previous constraint given by equation (3.5.15), it is theoretically possible to achieve ring gratings within the range of:

$$\frac{-m}{\tan\theta} > s > \frac{-2m}{\tan\theta} \qquad (3.6.11)$$

In this range of values, the geometry will never allow the reflected interfering beam to reach the centre of the circular SRG. This can be seen in Figure 3.11 where similar triangles PAQ and IAO are set by the condition that point A is twice the length from the origin as point Q where the extended line of the CDG mirror intersects the y-axis. In this case the reflected source beam is parallel to the CDG mirror and would therefore require an infinitely high CDG height h in order to create an interference pattern all the way to the centre of the SRG at the origin. For any values of s in between point A and Q as stated in equation (3.6.11), ring gratings are possible but a full circular grating will not be possible to create.

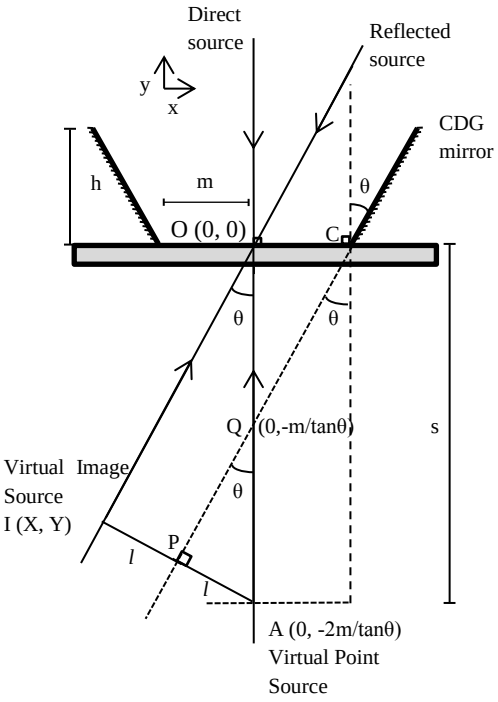

Figure 3.11 – Figure demonstrating the geometery of the maximum critical height for a CDG with a converging light source

CHAPTER 4: Experimental Procedure

4.1 Preparation of the Azo-glass samples

A Dispersed Red 1 (DR-1) azo-benzene compound with mexylaminotriazine group is synthesized according to literature[13]. The result is a fine powder which is prepared in a 3 percent solution, by weight, in dichloromethane. The solution is mixed by shaking for approximately one hour and then passed through a 50 μm filter. Glass microscope slides are cut into squares about 3 by 3 cm large. They are cleaned with soap and water, wiped dry and further air dried in an oven at 100 degrees Celsius for 10 minutes. The dry slides are blown with compressed air to remove any dust particles and are placed in a humidity-controlled chamber on a spin coater where approximately 3 ml of the prepared azo-glass solution is manually deposited and spun at 1500 rpm for 40 sec. The sample is then placed in an oven at 95 degrees Celsius for a further 20 minutes to evaporate any remaining solvent. The typical film thickness ranges from 400 to 500 nm as measured with a Sloan Dektak II D profilometer, model 139961. The sample films are then ready for inscription as detailed in the following sections.

4.2 Manufacturing and measuring of the CDG fixtures

Several CDG fixtures were machined and polished using manual equipment found in common machine shops. Care was taken to ensure that the reflecting conical surface was a true truncated cone, finishing at a knife-edge on the minor aperture, with its central axis perpendicular to the flat face. The material used was high-quality annealed carbon steel. After machining and polishing, the CDG fixtures were washed with solvent and dried with air. Approximately 500 nm of silver was then sputter coated onto each CDG in order to create a mirror-like finish on their interior surface. An example of a finished CDG is shown in Figure 4.1.

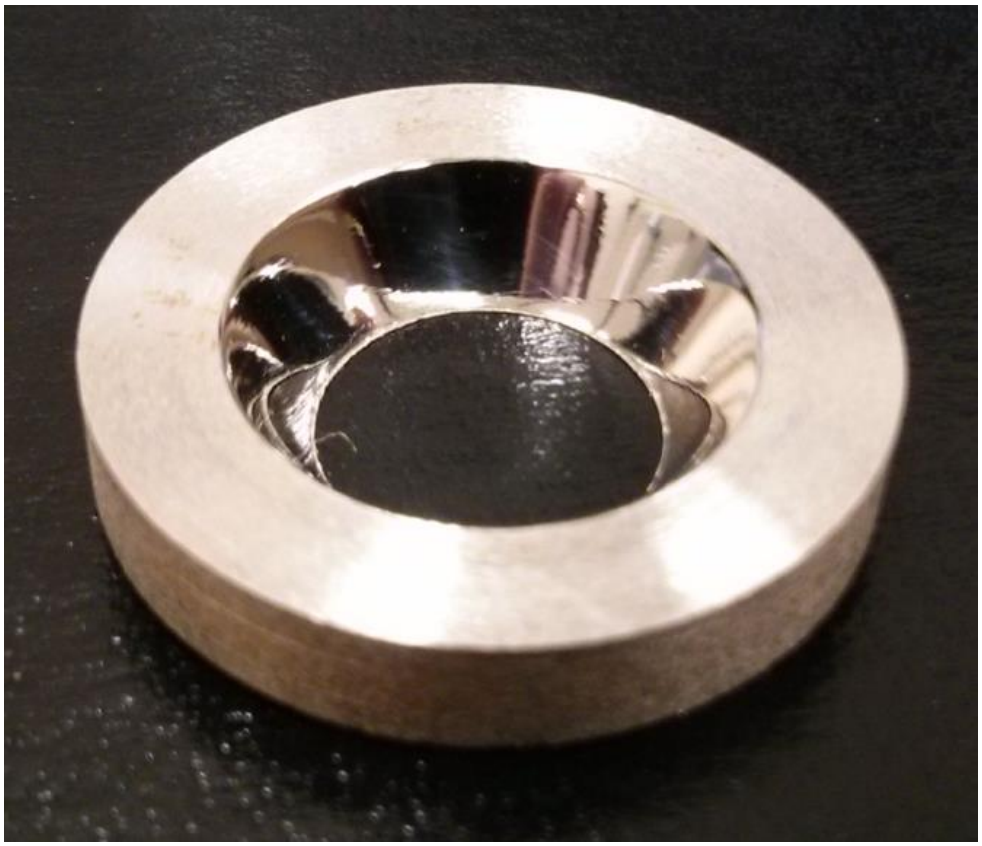

Figure 4.1 – A Circular Diffraction Grating Generator or CDG for short.

A total of six CDGs were manufactured with nominal angles θ of 12, 20, 25, 30, 32.5 and 42.5 degrees. The height, h, and the radius of the minor aperture, m, of the CDGs were measured using digital callipers with an instrument uncertainty of 0.02mm. The width of the CDG mirror, t, was measured using a travelling microscope with a Vernier scale accurate to within 0.02mm. Because of the somewhat subjective nature of the measurements taken with the travelling microscope, 3 trials were performed to estimate the average value and random uncertainty, which was added to the instrument error. The angle θ was calculated by using the inverse tan of t divided by h as in Figure 3.9. The error in the measured angle was calculated using the partial differential method. Since the tolerances of the machining process are not known, the measured angles and errors seen in Table 4.1 are used in all graph data and theoretical calculations in this thesis.

Table 4.1 – Nominal and measured CDG angles. The measured angles are taken for the remainder of this thesis. The row in bold corresponds to the CDG geometry used for chirped circular grating portion of the experiment.

Nominal CDG angle (degrees)	Width of CDG mirror in radial axis: t (mm)					Height of CDG mirror: h (mm)		Measured CDG angle: θ (degrees)	
	trial 1	trial 2	trial 3	average	error	value	error	value	error
42.5	3.91	3.88	4	3.93	0.08	4.62	0.02	40.4	0.7
32.5	2.58	2.68	2.66	2.64	0.07	4.5	0.02	30.4	0.8
12	1.5	1.42	1.52	1.48	0.07	6.97	0.02	12.0	0.6
20	2.12	2.54	2.3	2.32	0.23	6.58	0.02	19.4	1.8
25	3.42	3.32	3.76	3.5	0.24	7.55	0.02	24.9	1.6
30	**2.34**	**2.48**	**2.38**	**2.40**	**0.09**	**4.34**	**0.02**	**28.9**	**1.0**

4.3 Inscription of constant pitch circular gratings using a planar wave front

An azo-glass sample was placed directly on the reverse side of a CDG as in the experimental setup illustrated in Figure 4.2. The beam from a 5-watt Verdi diode-pumped laser (model 0174-525-52) with a wavelength of 532 nm was passed through a spatial filter, collimated with a convex lens, and circularly polarized by a quarter-wave plate. Circularly polarized light is used to ensure an even grating is formed in all directions of the circular SRG. Linearly polarized light directly from the laser would not work well for forming circular gratings because of the polarity dependence of the photo induced transport effect in azo-glass as mentioned in section 1.4. The resulting collimated beam was measured to have an irradiance of 604 mW/cm^2. The beam diameter was controlled by a variable iris and was projected onto the CDG and sample. All of the optical elements were mounted to a solid rail on an optical experiment table. Special care was taken to ensure that all optical elements were centred along the optical axis and the collimated beam was perfectly orthogonal to the CDG in order to match the theoretical geometry as accurately as possible.

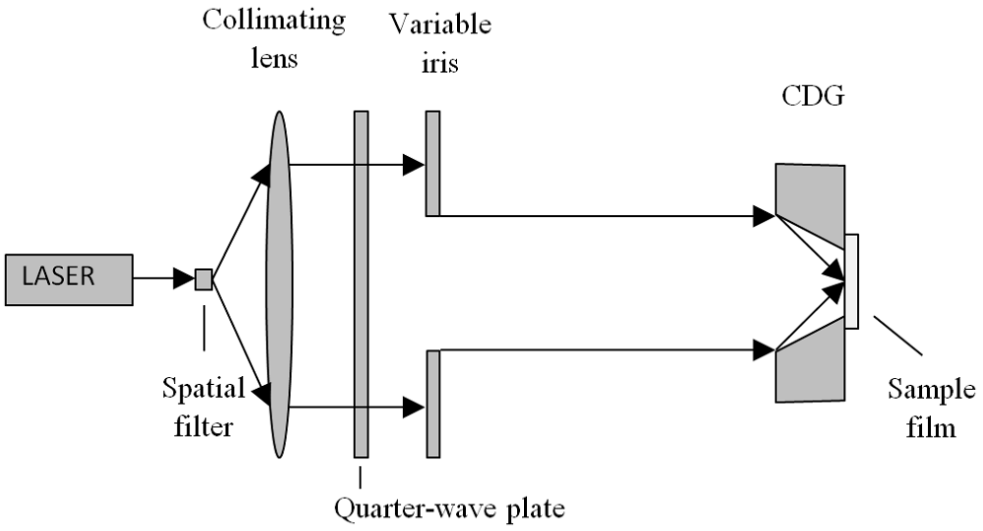

Figure 4.2 – Experimental setup for inscription of constant pitch circular gratings.

The real-time diffraction efficiency was measured as the SRG was forming by using the set-up depicted in Figure 4.3. A low-powered helium neon probe laser was aimed at the sample where the circular grating was being inscribed. The beam from the probe laser was mechanically chopped and a silicon photodiode was placed at the location of the first-order diffraction maximum. The signal from the photodiode was amplified by a lock-in amplifier and plotted as a function of time on a computer. The diffraction efficiency was calculated by dividing the power from the first diffraction order by the power from the incident beam, which was measured in a similar manner. This was done in order to verify the amount of laser exposure time required to generate the most efficient diffraction grating.

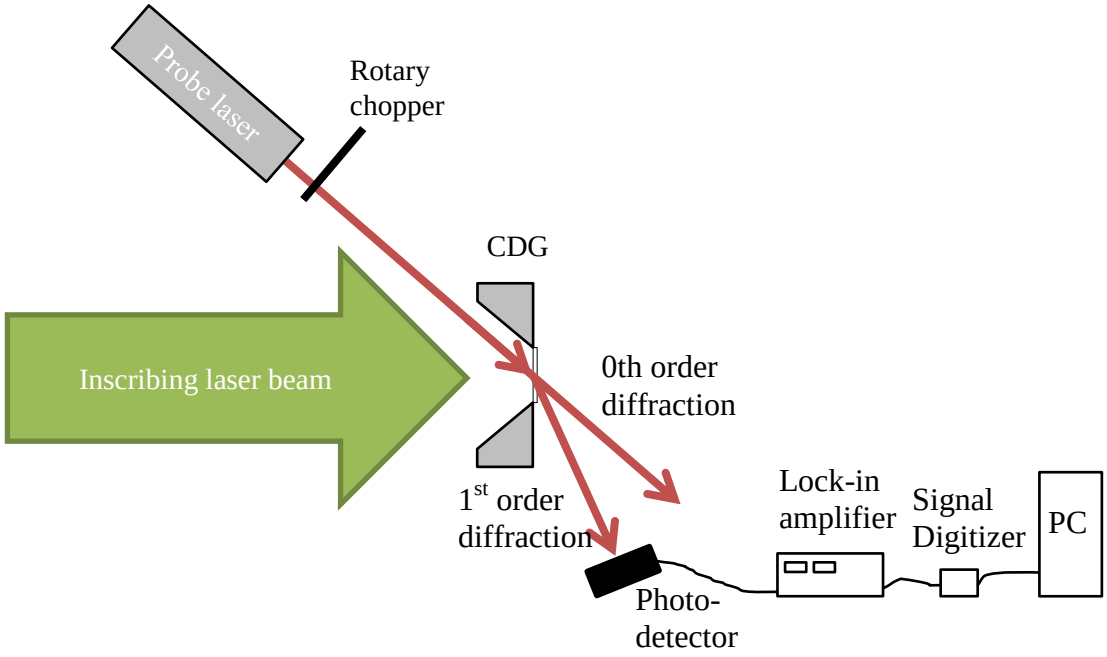

Figure 4.3 – Experimental set-up for measurement of real time diffraction efficiency of a grating as it is being photo-inscribed.

In total, five different SRGs were generated using the first five CDGs listed in Table 4.1. As outlined in section 3.7, the CDG must be shorter than the critical height h_c or the reflected light will cross the centre point of the circular grating and cause unwanted interference. However, the implications of changing the height of a CDG were not fully understood at the time that the CDGs were being manufactured. Table 4.2 shows the measured height compared to the theoretical critical height h_c. It can be seen that in some cases, large discrepancies exist between the ideal value of h_c and the measured height of the CDGs. These differences in measured height versus critical height can be mitigated in several ways. In the case where the measured height of the CDG was larger than h_c, the variable iris in the experimental setup was reduced in size. This effectively reduced the size of the beam reaching the outside edges of the CDG, and therefore eliminated any cross interference from happening. If the height of the CDG was too small, a ring grating was created, and good data points can still be taken in the ring portion of the grating. After the 5

SRGs were inscribed, their pitches were then measured using three independent measurement techniques.

Table 4.2 – Measured height compared to critical height for the 5 CDGs used in the collimated beam experiment. The critical height is calculated for a collimated laser source using equation (3.6.4).

Measured CDG angle - θ (degrees)	Minor radius - m (mm)	CDG Height - h (mm)	
		measured	h_c
40.4	5.65	4.62	1.06
30.4	5.60	4.5	4.66
12.0	5.72	6.97	24.61
19.4	5.72	6.58	12.64
24.9	5.92	7.55	8.25

4.4 Measurement techniques for grating pitch

Atomic Force Microscope (AFM) measurements of the grating pitch were taken using a Pacific Nanotechnology Nano-R O-020-0002 scanning probe microscope that was calibrated to be within 3% accurate using a sample with known dimensions. The grating pitch was measured from the AFM imagery over the maximum number of visible grating periods and then averaged to improve accuracy of the results. Four separate scans were also made on each circular grating at 0, 90, 180, and 270 degree positions and these results were further averaged.

A set of circular SRGs produced from each CDG were sputter coated with approximately 60 nm of gold. A Philips CP-XL30 Scanning Electron Microscope (SEM) with an instrument uncertainty of 5% was then used to create imagery of the coated SRGs with magnifications less than capable by the AFM in order to view a larger portion of the grating. The length of ten grating periods was measured from the digital images using public domain imagery software ImageJ[h]. The results were divided by ten to achieve an average measurement of the grating pitch.

The final measurement method for estimating the grating pitch of the circular SRGs is by performing direct measurements of the diffraction angle. A 4 mW helium neon laser,

[h] ImageJ software by Wayne Rasband. National Institute of Mental Health, Bethesda, Maryland, USA. http://imagej.nih.gov/ij/

semi-transparent beam splitting mirror and computer controlled rotary table were placed on an optical experiment table in the configuration shown in Figure 4.4. Prior to the diffraction grating being inserted, a screen is marked with a vertical line to indicate the position of the laser beam as it passes straight through the system. The rotary table with attached sample diffraction grating is then rotated until the zeroth reflected diffraction, which is also reflected off the beam splitter, is aligned with the vertical screen marking. This indicates that the light beam is normally incident on the sample. The rotary table is then turned until the first reflected diffraction order is reflected off the beam splitter and aligned with the line on the screen. In this position of the rotary table, the diffracted beam is travelling along the same path as the incident beam, so therefore, the angle of incidence is equal to the angle of diffraction. The computer calculates the difference in angle from the normal position to the angle that this occurs. Using equation (3.3.22) and given the first diffraction order m = 1 as well as given that $\theta_1 = \theta_i$ leads to the equation:

$$\Lambda = \frac{\lambda}{2\sin\theta_1} \qquad (4.3.1)$$

Knowing the wave length of the laser and with value of θ_1 from the rotary table allows for the precise calculation of the pitch Λ. Measurements are taken from the 1 and -1 diffraction orders and the results are averaged to further improve the precision of the measurement.

The grating equations, and subsequently equation (4.3.1), are derived using a linear array of point sources, and so technically speaking these equations should apply to linear diffraction gratings. However, if the laser from the diffraction measurement set-up illuminates a small portion of a circular SRG near the outside edge of the grating, then this small region of the circular grating is a good approximation of a linear grating. This is because size of the grating pitch (and the illuminated test region) is very small compared to the overall radius of the circular grating. Therefore the pitches calculated by this direct diffraction angle measurement method remain valid approximations.

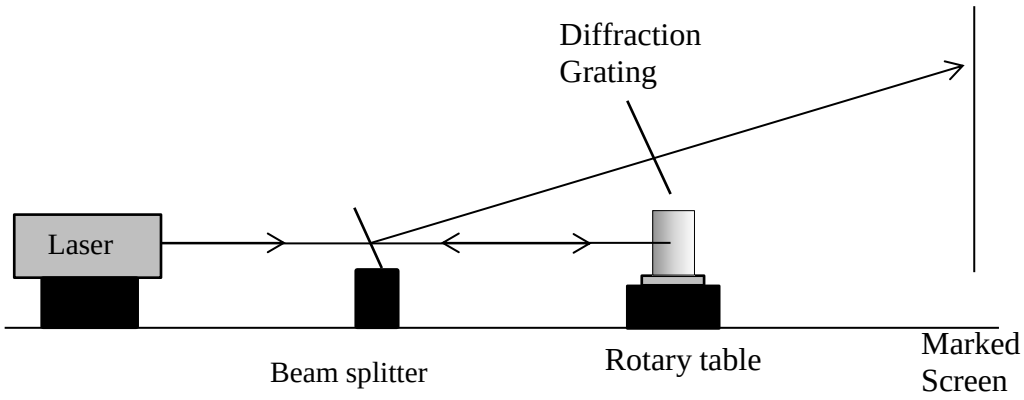

Figure 4.4 – Side view of the direct diffraction angle measurement set-up used to calculate grating pitch.

4.5 Inscription of chirped pitch circular gratings with a curved wave front

The experimental setup for inscribing chirped pitch circular SRGs is very similar to the setup described in section 4.3. However, in this case a focusing lens is inserted into the optical path between the variable iris and the CDG. Because the incoming light is collimated, the focusing lens generates an approximation of a point source of coherent light at its focal point. Depending on the focal length of this lens and the distance to the sample film, the point source may be used to produce a diverging or converging spherical wave front as illustrated in Figure 4.5. A lens with a focal length of 5 cm was used for the diverging case, while a lens with a focal length of 30 cm was used in the converging case. A rail-mounted screen was used to find the location of the point source in order to verify the distance, s, between the point source and the sample.

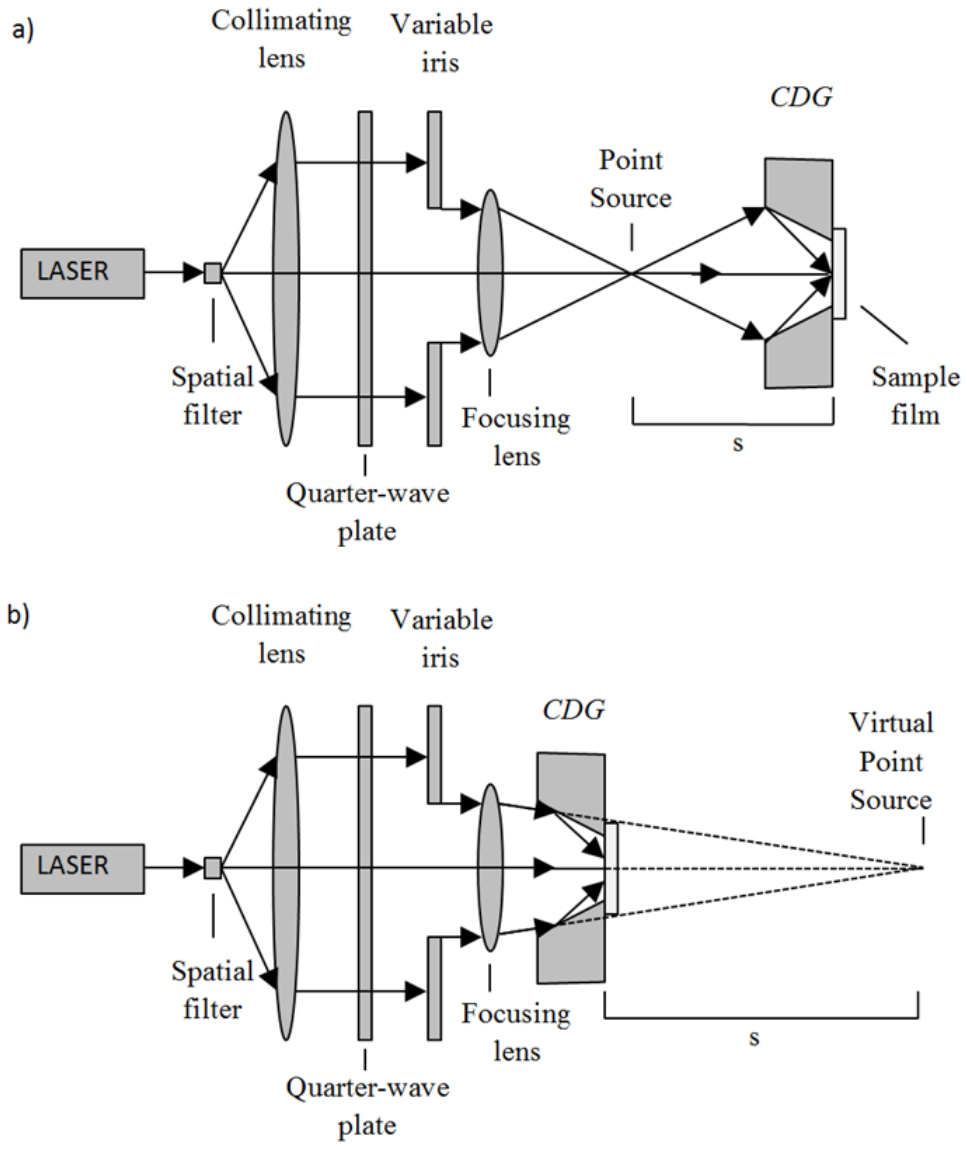

Figure 4.5 – Experimental setups for inscription of chirped pitch circular gratings. (a) Representation of the case where the focal point of the focusing lens is placed ahead of the CDG to create a diverging source. (b) Representation of the case where the focal point of the focusing lens is placed behind the CDG to create a converging source.

In this portion of the experiment only one CDG with a measured angle of 28.9 degrees was used. Its dimensions are specified in the row in bold from Table 4.1. Multiple trials were performed with different distances, s, between the point source and the sample in order to better understand the effects of this parameter on the resulting SRG. Because of constraints in the length of the optical rail, and because of interference between rail-mounted optical elements, five values of s were used: -20, -10, 3, 6, and 9 cm.

Again, as discussed in the theory section, the critical height of the CDG must be considered. This time because the inscribing light has a spherical wave front, the critical height of a given CDG changes with the distance to the point source, s, as described in section 3.7. Table 4.3 shows this theoretical relationship using the same experimental geometry outlined in this section. The additional theoretical cases of s = 1000 cm and s = -1000 cm were added to this table to demonstrate that for large absolute values s, the calculated values of h_c for a spherical wave front approach the theoretical value of h_c = 5.73 mm for a collimated source. This indicates that the derived theory for critical height of the CDG is self-consistent because distant point sources can be approximated as collimated light.

Table 4.3 – Critical height of a CDG as the distance from the sample to point source (s) varies. These values were calculated using equation (3.6.8) with CDG angle of 28.9 degrees and minor aperture radius of 5.95 mm. The critical height of the CDG for a curved wave front approaches the value for the critical height of the CDG for a collimated wave front, h_c = 5.73 mm, for large absolute values of s.

Distance from point source to sample: s (cm)	Critical height of CDG for curved wave front: h_c (mm)
1000	5.71
9	4.13
6	3.55
3	2.28
-10	7.99
-20	6.72
-1000	5.74

The actual measured height of the CDG was 4.34 mm. In the cases where the actual height was larger than the required h_c from Table 4.3, the variable iris was reduced in size, effectively reducing the size of the CDG exposed to light. This was done conservatively in order to ensure no crossover interference would take place. According to theory, the result is that the gratings would not be formed all the way to the centre of the circular SRG but instead would form a band of grating grooves in the shape of a ring of concentric circles. Similarly, when the measured height of the CDG was smaller than the required critical height, ring gratings were also formed. The pitch of the resulting SRGs was then measured at various distances from the centre of the grating order to determine the profile of the chirp of the grating pitch. Because ring diffraction gratings were formed, not full circular gratings, the

pitches were measured from the edge of the grating to as close to the centre of the grating as measurements would allow.

For the chirped pitch gratings, the AFM was the only instrument used to measure grating pitch as a function of position. This instrument has already been proven to be an accurate form of measurement from the experiments with constant pitch circular gratings. The very small scanning area for the imagery combined with the ability to accurately control the sample position on a sub-millimetre scale using the computer controlled sample platform, made the AFM an excellent tool for this application. Direct diffraction angle measurements would have been problematic because of the larger sample area covered by the probe laser beam and because of difficulties with measuring the distance from the centre of the circular grating. SEM imagery would have offered a good alternative to the AFM measurements but its operation was dependent on technician availability where the AFM measurements could be done in-house.

CHAPTER 5: RESULTS

5.1 Results from the real time diffraction efficiency measurements

Real-time measurements of the diffraction efficiency of circular SRGs were taken as they were being inscribed, as described in section 4.3. The resulting graph of the diffraction efficiency as a function of time is shown in Figure 5.1. This figure shows a smooth increase in the diffraction efficiency of the grating after the inscribing laser is turned on at t=0. The graph plateaus at approximately t=300 seconds when the maximum grating height is reached. The large downward spike just after t=600 seconds occurred when the inscribing laser was turned off since the sudden change in illumination took a few cycles for the lock-in amplifier to average out the signal. Based on the results of this graph, an exposure time of 350 seconds was chosen for subsequent production of circular SRGs in this experiment.

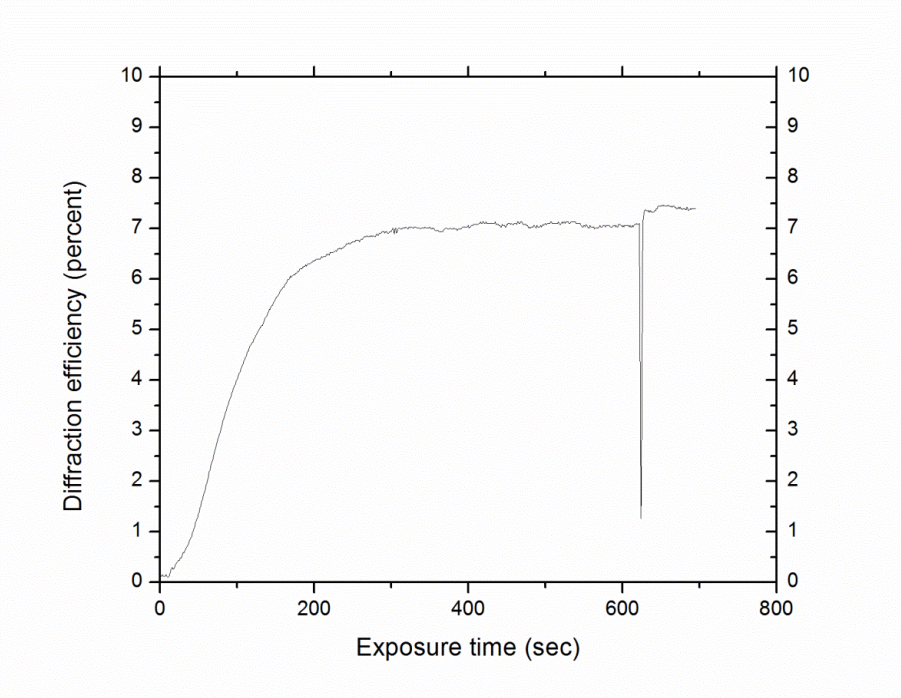

Figure 5.1 – Real-time first order diffraction efficiency of a circular SRG as it is being inscribed in DR-1 azo-glass by a 40.4 degree CDG using a collimated laser beam with an irradiance of 604 mW/cm^2

Because the SRG being formed is a circular grating, the first order diffraction maximum from the probe laser is an arc of a circle instead of a point as with a linear grating. The photo-sensor used to measure the relative power was placed as close as possible to the sample in order to capture as much of the light from the diffraction order as possible, however some of the light fell outside of the sensor area. The result is that the calculated diffraction efficiency shown in Figure 5.1 may be lower than the true diffraction efficiency. However this inaccuracy was deemed acceptable, since the main purpose of collecting this data was for determining the amount of exposure time required to inscribe gratings using the experimental set-up. The data in graph Figure 5.1 may not be the true absolute diffraction efficiency, but still demonstrates the amount of time required in order to maximize the grating efficiency.

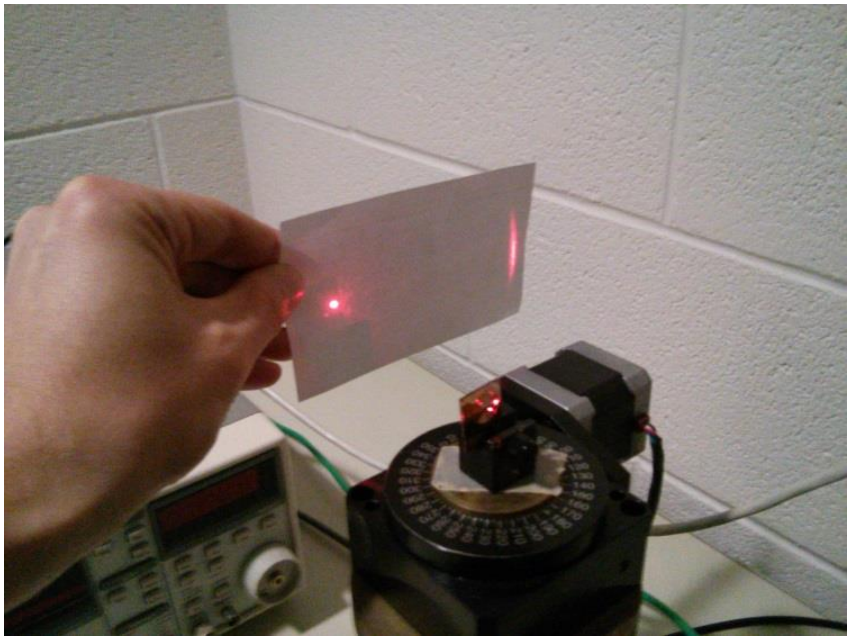

Figure 5.2 – The first order diffraction maximum is an arc of a circle when a small portion of the circular SRG is illuminate by a probe laser. This makes calculations of the diffraction efficiency more difficult since not all of the diffracted light can be captured on the surface of the photo-sensor.

5.2 Results from constant pitch circular SRGs produced with planar wave fronts

A grating produced as outlined in section 4.3 is shown in Figure 5.3. Although the resulting gratings appeared to be circular, the individual grating lines themselves are much too small to be seen with the naked eye. In order to verify that circular gratings were

produced, one of the SRGs was exposed to a low power Helium Neon laser with a collimated beam that illuminated the entire grating surface. The resulting diffraction pattern is shown in Figure 5.4. The zeroth order is the circle in the centre where light passes straight through the grating. The first order maximum is represented by the ring of light and is consistent with the pattern expected from a circular diffraction grating. This diffraction pattern also demonstrates that the experimental set-up has recorded an accurate holographic representation of the incident and reflected inscribing light from the CDG, and is able to reproduce this pattern holographically when illuminated with monochromatic light.

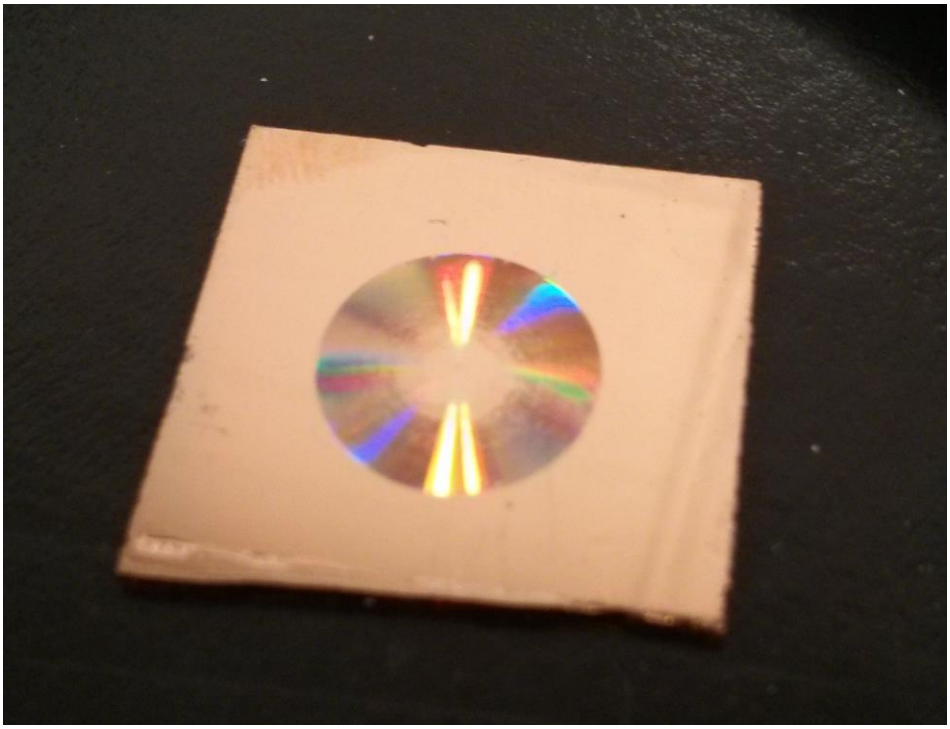

Figure 5.3 – A circular SRG with radius of approximately 11mm produced holographically using a CDG. This sample has been coated with gold prior to observations being made with a SEM. It can be seen that the grating pattern does not reach all of the way to the centre of the SRG, but forms a band of rings. This was done intentionally in order to ensure no cross over interference occurred from the opposite side of the CDG.

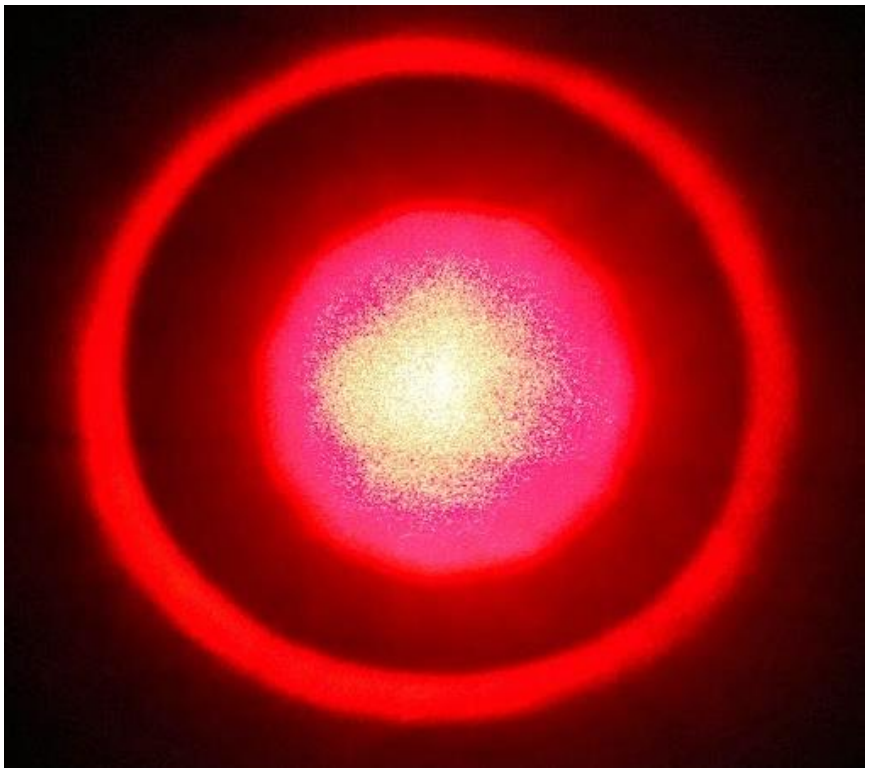

Figure 5.4 – A photograph of the diffraction pattern produced from a circular SRG being completely illuminated by a low-powered collimated laser beam. The screen is approximately 1 cm away from the grating and shows the zeroth and first order diffraction pattern consistent with a circular diffraction grating.

The five different sample gratings were then imaged using an AFM. An example of imagery from the AFM is shown in Figure 5.5. This figure shows a regular sinusoidal grating pattern with the grating grooves aligned in the azimuthal direction, consistent with an SRG made up of concentric rings. The maximum measured grating depth was approximately 250 nm.

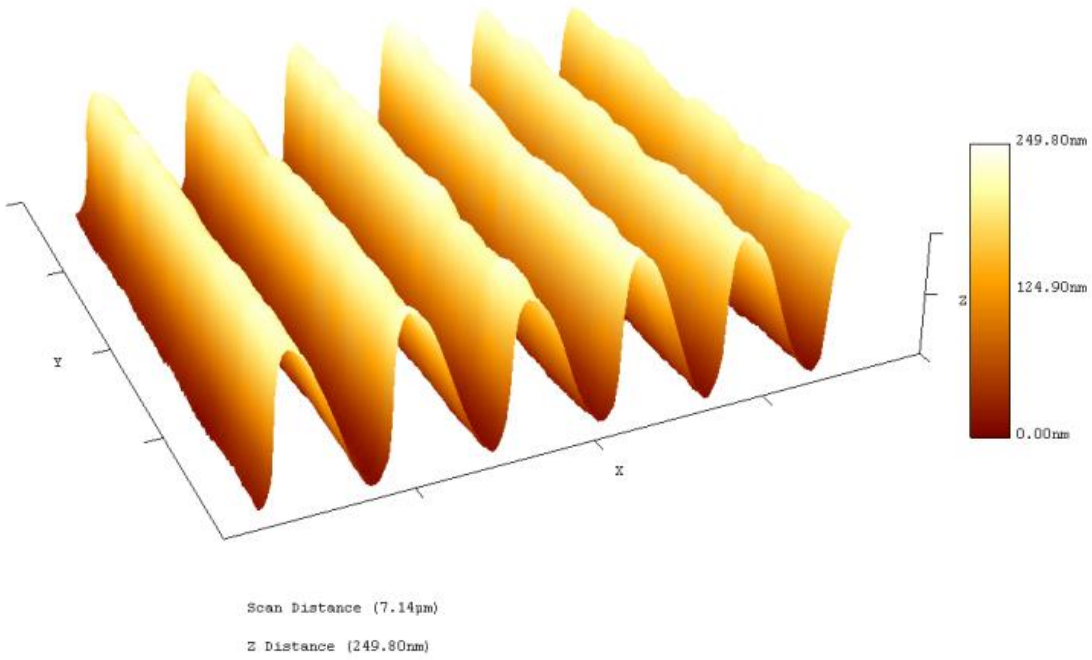

Figure 5.5 - AFM scan of circular SRG generated by a 19.4 degree CDG. The x-axis corresponds to the radial direction of the circular grating while the z-axis is the depth of the SRG. The average grating pitch measured from four different AFM scans at the 0°, 90°, 180° and 270° positions of this grating was 905 nm.

Table 5.1 shows the results of pitch measurements taken from the AFM scans. Because the AFM has a very small scan area of about 7µm across, it is possible to see some localized differences in grating pitch, possibly caused by imperfections in the CDG mirror or slight misalignment of the optical elements in the experiment. For this reason, four scans were taken of each circular SRG at 0, 90, 180 and 270 degree positions. These results were then averaged for the final value. Random uncertainties of the grating pitch were calculated by subtracting the smallest measured value from the largest measured value and dividing by 2 for each circular SRG. The random uncertainty was then added to the 3% instrument uncertainty to give a total uncertainty to the measured pitch. The theoretical values of grating pitch were calculated using equation (3.4.11) and a wavelength of 532nm. All theoretical results of grating pitch fall within the uncertainty of the measured pitch.

Table 5.1 – Theoretical results compared to measured results from AFM scans of grating pitch for five circular SRGs made from CDGs with different angles. Theoretical pitches were calculated using equation (3.4.11).

Measured angle of CDG (degrees)	Theoretical prediction of grating pitch (nm)	Grating pitch as measured by AFM scan (nm)					
		90^{o} position	180^{o} position	270^{o} position	0^{o} position	**average**	Uncertainty (instrument + random)
40.4	**539.0**	580.9	556.3	569.1	548.8	**560**	30
30.4	**609.5**	629.7	614.0	638.9	616.3	**620**	30
12.0	**1309.2**	1309.8	1495.0	1475.0	1314.6	**1400**	140
19.4	**848.2**	925.3	894.0	934.2	866.6	**900**	60
24.9	**697.1**	719.3	722.9	771.0	718.7	**730**	50

At the time that the SEM was available, the CDG with an angle of 24.9 degrees had not yet been manufactured. For this reason it was only possible to take SEM imagery of four out of the five SRGs. The four available samples were sputter coated with a thin film of gold and imagery was taken at various levels of magnification. Example SEM imagery is shown in Figure 5.6. At magnification levels of about 2000 times, the individual grating grooves can be resolved and appear to be consistent over large areas and very regularly spaced. The curvature of the circular grating lines cannot be easily seen because the level of magnification is still relatively high and their radius of curvature is relatively large so that the grating groves appear to be linear. At a magnification level of 15000 times, the individual grating lines are very clearly resolved and can be measured using the integrated scale on the images.

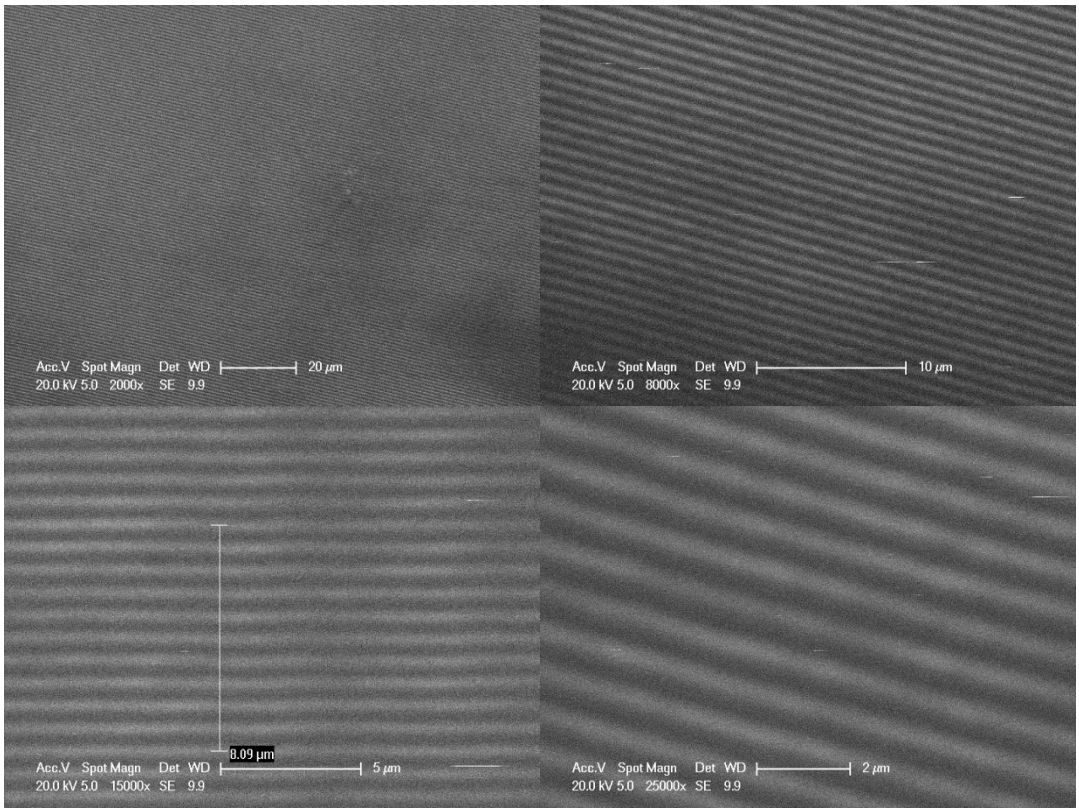

Figure 5.6 - SEM imagery of circular SRG generated from a 19.4 degree CDG over a range of magnification powers. At 2000 times magnification, the grating peaks can be visually resolved showing a highly regular grating pattern over a scale of about 100 µm. At 8000, 15000, and 25000 times magnification grating lines are very clear. The distance of 10 lines is measured to give an average pitch of 809 nm.

Table 5.2 shows the theoretical grating pitches compared to the pitches measured by the SEM imagery. It was not possible to take multiple images at different locations of the SRGs using the SEM because of time constraints, so the random uncertainty is not known. However by using an instrument uncertainty of 5%, all of the predicted theoretical grating pitches fall within the uncertainty of SEM measurements.

Table 5.2 - Theoretical results compared to measured results from SEM imagery of grating pitch for four circular SRGs made from CDGs with different angles. Theoretical pitches were calculated using equation (3.4.11).

Measured CDG angle (degrees)	Theoretically predicted grating pitch (nm)	Average measured pitch from SEM (nm)	SEM instrument uncertainty: 5% (nm)
40.4	539.0	540	30
30.4	609.5	580	30
12.0	1309.2	1280	60
19.4	848.2	810	40

The final method used to measure the grating pitch of the constant pitch circular SRGs was to measure the angle of diffraction of the first order maxima as described in section 4.3. A computer program controls the rotary table, measures and records the diffraction angle, and automatically performs the required calculations using equation (4.3.1). The resulting pitch measurements are shown for SRGs from all five CDG angles in Table 5.3 and it can be seen that the measured pitches fall within the uncertainty of the predicted values.

Table 5.3 - Theoretical results compared to measured results of grating pitch calculated from diffraction angle measurements for five circular SRGs made from CDGs with different angles. Measured pitches were calculated using equation (4.3.1) and theoretical pitches were calculated using equation (3.4.11).

Measured CDG angle (degrees)	Theoretically predicted grating pitch (nm)	Pitch calculated from diffraction angle (nm)	Calculated Pitch uncertainty: 5% (nm)
40.4	539.0	540	30
30.4	609.5	610	30
12.0	1309.2	1270	60
19.4	848.2	830	40
24.9	697.1	710	40

A graph summarizing the measured grating pitches from all three measurement techniques compared to the theoretically predicted value is shown in Figure 5.7. Uncertainty in the CDG angle for each point is taken from Table 4.1. It can be seen that the results for all three independent methods of measuring grating pitch are consistent and agree well with the predicted value from equation (3.4.11).

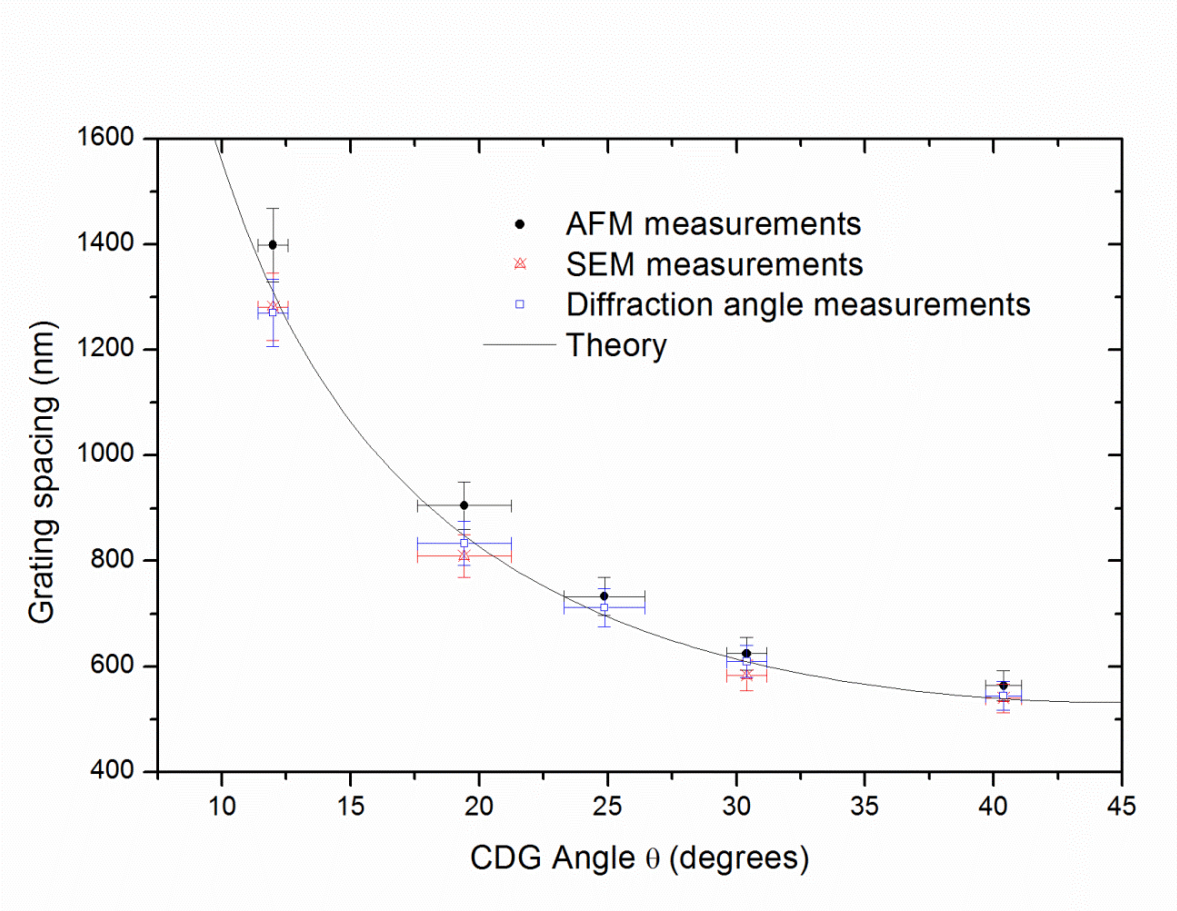

Figure 5.7 - Theoretical and measured results of the SRGs pitch inscribed by a 532 nm laser as a function of CDG mirror angle θ. Measured results include data points taken from AFM, SEM and direct diffraction angle measurements. The theoretical curve is plotted using equation (3.4.11).

5.3 Results from chirped pitch circular SRGs

AFM scans were taken of the 5 chirped pitch circular SRGs that were generated from the 28.9 degree CDG with different distances to the point source of light. An example of the AFM imagery taken is seen at Figure 5.8. The scans were taken approximately every 0.5 mm along a randomly chosen radial line starting at the outside edge of each circular SRG. The scans were also repeated at the same distance from centre, δ, but on the opposite side of the SRG. The grating pitch was measured from the imagery by averaging the distance between multiple grooves. This result was then averaged again with the results from the AFM imagery taken from the opposite side of the SRG. Grating pitch data as a function of δ as measured by the AFM imagery is presented as black points in Figure 5.11 through Figure

5.15. Uncertainty in the pitch was calculated by taking the absolute value of the difference between the two trials divided by two to find the random uncertainty and adding this to the 3% instrument uncertainty.

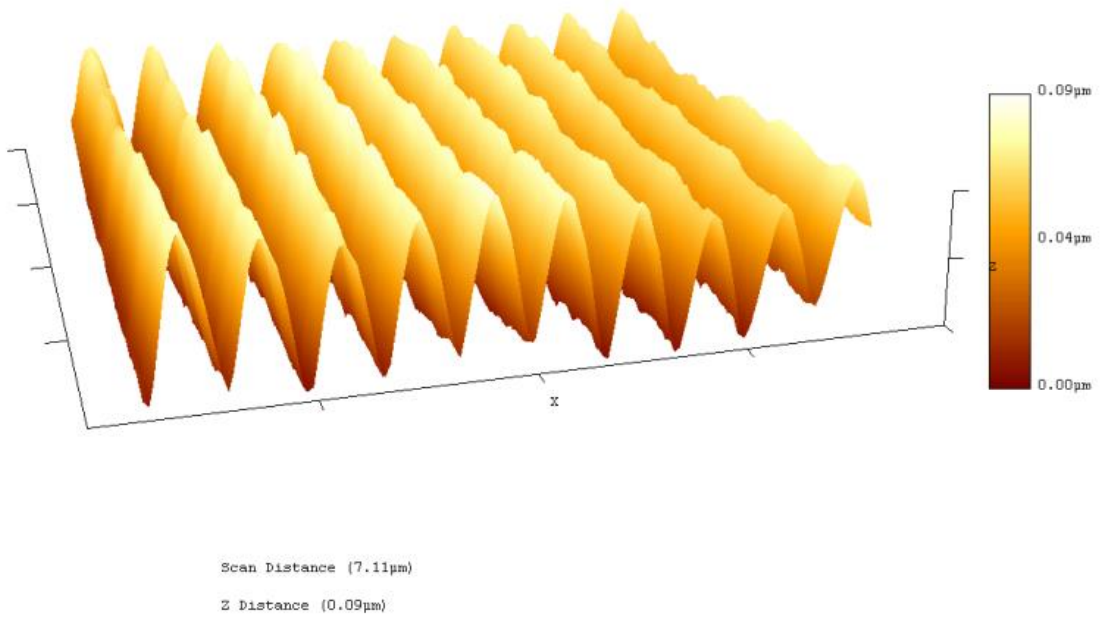

Figure 5.8 - AFM imagery at 1mm from the edge of a circular SRG inscribed using a 28.9 degree CDG with a point source of inscribing light at s = -10 cm.

The computer ray trace simulation described in section 3.6 was used in order to provide a theoretical solution to compare with the collected data. The ray trace simulation provides two main outputs: a cross sectional schematic of the rays, as well as data points for the calculated pitch as a function of distance from centre of the circular SRG. Figure 5.9 and Figure 5.10 are two examples of schematics generated by the simulation that represent the calculated ray paths. Firstly, lines are drawn to represent the innermost and outermost beams that will strike the CDG and that are reflected in order to determine the angular boundaries of the simulation. Then, at a chosen interval, intermediate sample beams are drawn and are reflected by the CDG. Finally lines that represent beams of directly incident light are drawn to meet the points of the reflected intermediate sample beams. This output is used to visually confirm that the geometry of the simulation is working correctly. The fact that all of the

critical heights used in the simulation runs strike the centre point (δ=0), as seen in Figure 5.9 and Figure 5.10, and are in agreement with the critical heights taken from Table 4.3 adds further evidence to the accuracy of the simulation.

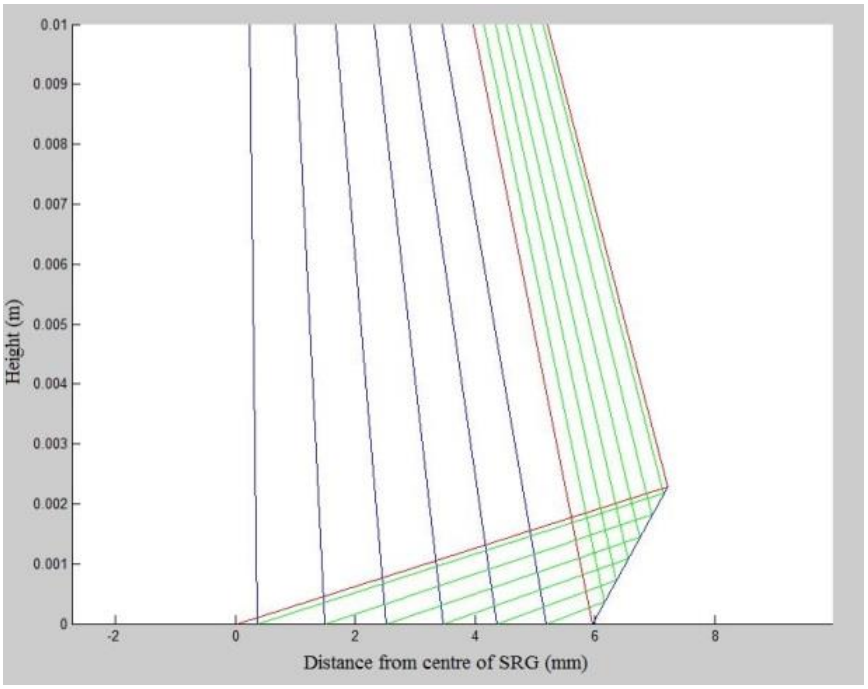

Figure 5.9 – Schematic of rays of light reflecting off of a 2D cutaway of a CDG mirror for a diverging wave front. The schematic is from the ray trace simulation using a distance to point source of s=3cm and a critical height of the CDG h_c=2.28 mm with the outermost reflected beam striking the centre of the SRG as predicted.

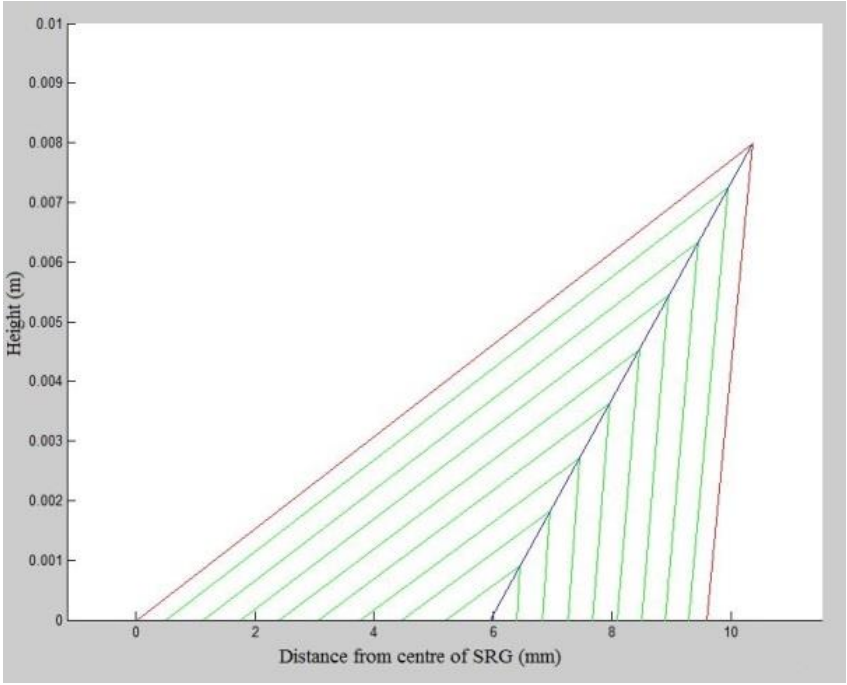

Figure 5.10 - Schematic of rays of light reflecting off of a 2D cutaway of a CDG mirror for a converging wave front. In this case it appears that the rays are coming from below the CDG. The reason for this is that it was convenient in the simulation to calculate the angle of incidence to the mirror, and subsequently the angle of reflection, by simulating the point of convergence as the true source of light. In the physical experiment the light is actually approaching from above and converging on a virtual point source below the sample. The schematic is from the ray trace simulation using a distance to point source of s=-10cm and a critical height of the CDG h_c=7.99 mm with the outermost reflected beam striking the centre of the SRG as predicted.

An additional result from the simulations is a graph with data points for the theoretical grating pitch as a function of δ, the coplanar distance from the centre of the SRG. These data points were calculated using simulation parameters that matched the geometry measured from the physical experiments as closely as possible. The wavelength of light was entered as 532 nm to match the wavelength of the laser used. The critical height from Table 4.3 was used as the height parameter for each case in the simulation. A measured CDG angle, θ, of 28.9 degrees from Table 4.1 and a minor radius of 5.95mm from Table 4.3 were used. Since there is an uncertainty of $\pm$1 degree in the measured angle, the simulation was also executed for CDG angles of 27.9 and 29.9 degrees. This was done for all five tested distances, s, from the point source to the sample film. These results can be seen as the solid, dashed, and dotted line graphs in Figure 5.11 through Figure 5.15. The red and blue lines border an area that represents a range of theoretical solutions within the confines of the error

in the CDG angle parameter. The black dotted line represents the ideal theoretical solution for a CDG angle of 28.9 degrees.

One additional step was taken in order to demonstrate that the theoretical grating pitches generated by the simulation were accurate. Although equation (3.5.7) does not simplify well in its general form, it can be approximated using numerical methods for specific cases. By assigning the same parameters to this equation as in the computer simulation and only leaving the values of PD and δ as variables, a solution was found for various test points using commercial algebra software to satisfy equation (3.5.9). By subtracting the solution values of δ_2 and δ_1, the pitch Λ can be found for each test point. This method was used to calculate grating pitches for various test values of δ, using the same distances from the point source to the sample, s, as used in the experiments. This was done using the same geometric parameters as the simulation. The results from this numeric solution can be seen as white circle points on Figure 5.11 through Figure 5.15. The results indicate a perfect agreement between the simulation and the numeric solution adding further confidence that the ray trace simulation is performing as expected.

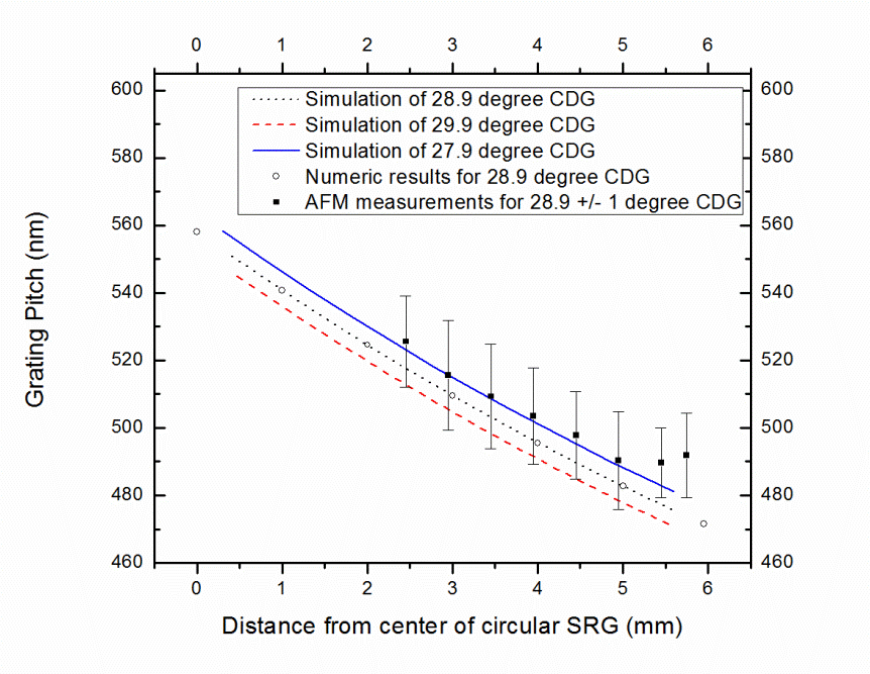

Figure 5.11 - Theory and measurements for a circular SRG inscribed from a 28.9 degree CDG with diverging point source 3 cm away from sample.

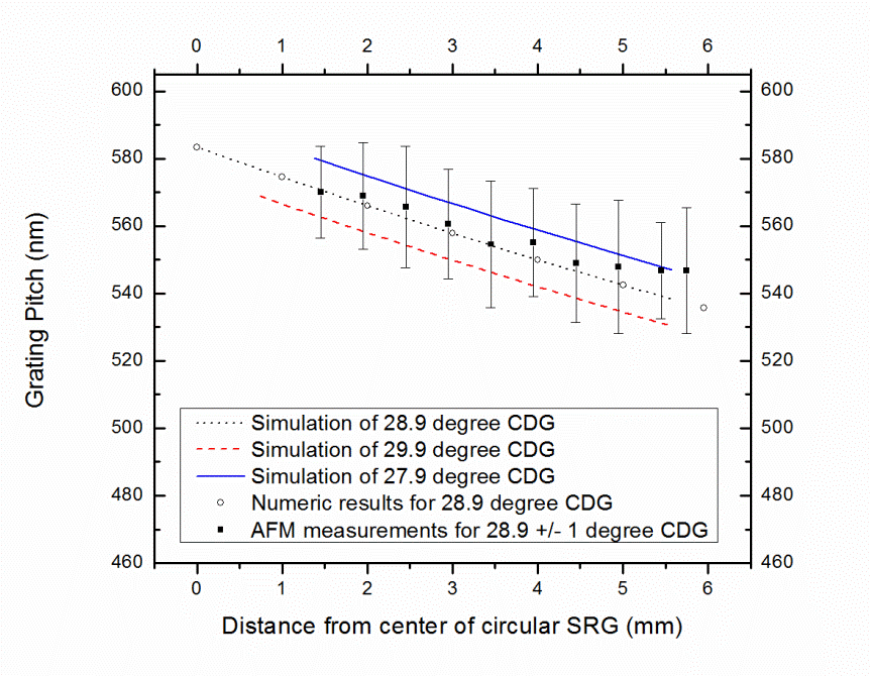

Figure 5.12 - Theory and measurements for a circular SRG inscribed from a 28.9 degree CDG with diverging point source 6 cm away from sample.

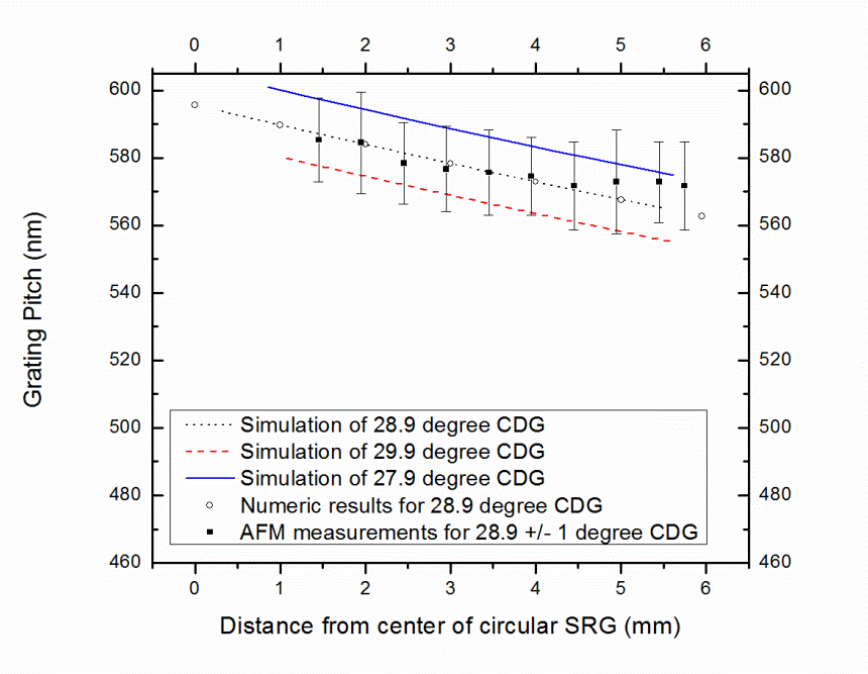

Figure 5.13 - Theory and measurements for a circular SRG inscribed from a 28.9 degree CDG with diverging point source 9 cm away from sample.

Figure 5.11 through Figure 5.13 represent the test cases where diverging light from the inscribing laser was used to inscribe chirped pitch SRGs. All three graphs have a negative slope indicating that the grating pitch gets smaller towards the edge of the circular SRGs. These three graphs show a general trend where the smaller the distance, s, to the point source, the more pronounced the chirp of the grating pitch. Figure 5.11 corresponds to data taken using a value of s = 3 cm and has the most pronounced negative chirp of -13.4 nm of pitch per mm of grating. Figure 5.12 corresponds to s = 6cm and has a chirp of -7.0 nm/mm. Figure 5.13 corresponds to a value of s = 9cm, and has the least amount of negative change in pitch over the surface of the grating at -4.5 nm/mm.

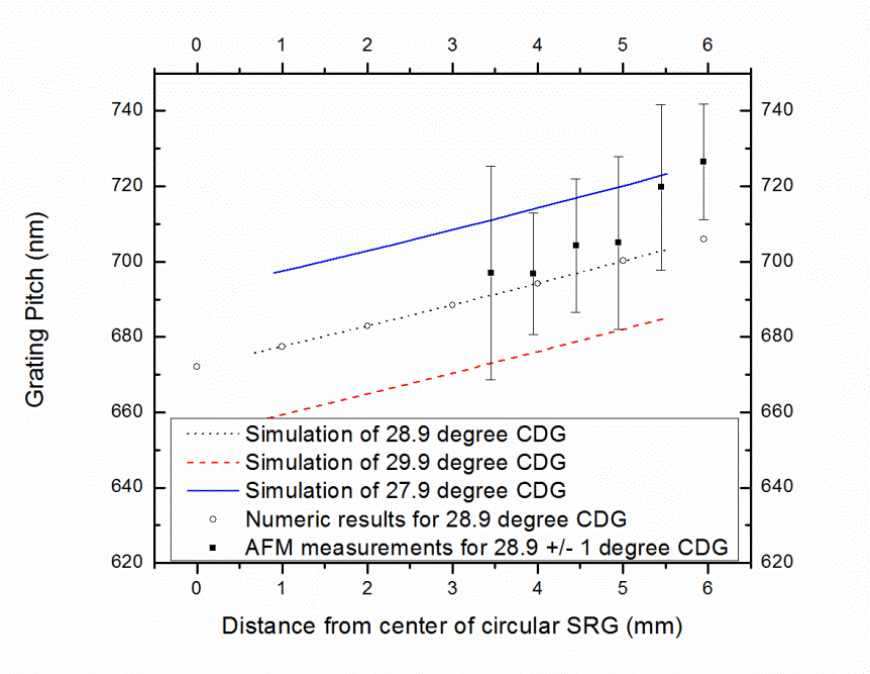

Figure 5.14 - Theory and measurements for a circular SRG inscribed from a 28.9 degree CDG with converging point source -10 cm away from sample. AFM measurements are not made for the values of δ smaller than about 3.5 mm because the height h of the CDG prohibits the formation of grating lines in the center of the SRG as discussed in section 4.5.

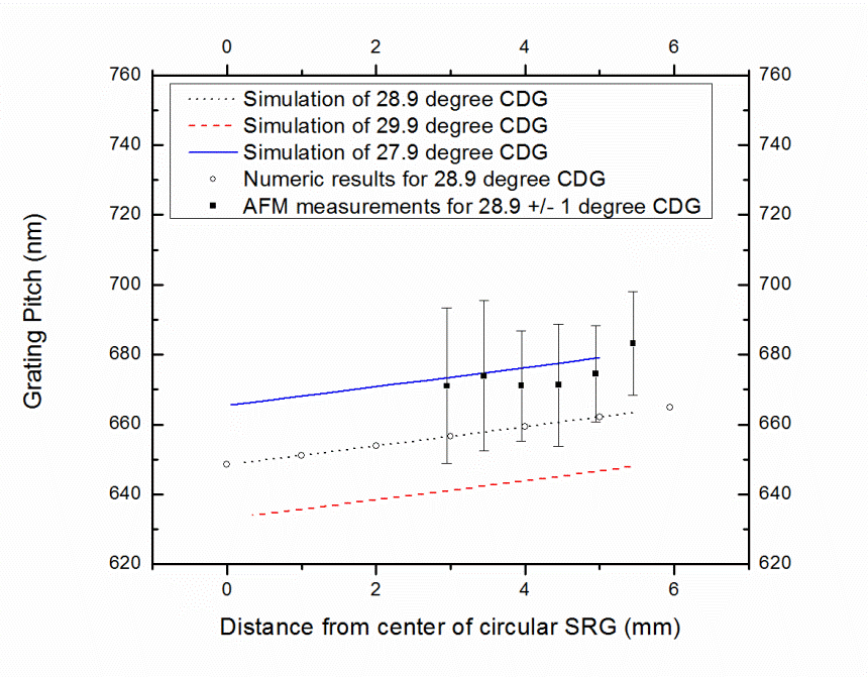

Figure 5.15 - Theory and measurements for a circular SRG inscribed from a 28.9 degree CDG with converging point source -20 cm away from sample. AFM measurements are not made for the values of δ smaller than 3 mm because the height h of the CDG prohibits the formation of grating lines in the center of the SRG as discussed in section 4.5.

Figure 5.14 and Figure 5.15 represent the test cases where converging light from the inscribing laser was used to inscribe chirped pitch SRGs. These two graphs have a positive slope indicating that the grating pitch gets larger towards the edge of the circular SRGs. Similar to the case of a diverging source, these graphs show a general trend where the smaller the distance, s, to the point source, the more pronounced the chirp of the grating pitch. Figure 5.14 corresponds to a value of s = -10 cm and has the most pronounced positive chirp of 6.3 nm of pitch per mm of grating. Figure 5.15 corresponds to a value of s = -20 cm, and has the least amount of change in pitch over the surface of the grating at 3.6 nm/mm.

A summary of the measured rate of chirp dependent on the distance, s, to the point source can be seen in Table 5.4. These values were calculated as the slope from linear regressions of the experimental data points.

Table 5.4 – Rate of change in grating pitch over distance from centre of chirped SRG for the 5 tested distances to the inscribing point source. Note that negative values of s correspond to a converging source where positive values of s correspond to a diverging source.

Distance from point source to sample – s (cm)	Rate of change in pitch over distance from centre of grating – Chirp (nm/mm)
-20	3.6
-10	6.3
3	-13.4
6	-7.0
9	-4.5

The experimental data points from Figure 5.11 to Figure 5.15 generally fall within uncertainty of the ideal theoretical solution of a 28.9 degree CDG. The differences between experimental and theoretical results can be accounted for by a number of potential sources for error. Any imperfections in the CDG mirror surface or in the alignment of the CDG or point source can alter the results. In order to help mitigate these sources of error, two measurements from opposite sides of the CDG were taken and the results averaged. Another source of error comes from the various parameters used in the simulation. Because of limitations in the accuracy of measuring the CDG angle using a travelling microscope, the relative uncertainty was highest for this parameter. This is the reason that several simulations were run to quantify the possible range of errors caused by the uncertainty of the CDG angle. However, additional error could have been introduced from inaccuracies in the distance to the point source, s, or the size of minor aperture of the CDG, m. These values were known with greater accuracy since they were measured directly and so had a smaller relative uncertainty than the CDG angle. Lastly, changes to the room temperature in the laboratory can theoretically affect the piezoelectric actuators on the AFM which might affect the accuracy of the AFM imagery. The AFM was recalibrated at the beginning of each day of test measurements and any variations are accounted for in the 3% instrument error included in the total uncertainty of the AFM pitch measurements.

One common trend that was seen in Figure 5.11 through Figure 5.15 is that the last two or three measured pitches furthest from the centre of the circular SRG are higher than expected for each SRG. It is believed that the reason for this unexpected observation is a result of the manufacturing process of CDG fixture itself. After the CDG is machined, it was polished in a time consuming process that removed small amounts of material on the surface of the CDG in order to get rid of any scratches. Although extreme care was taken to polish the CDG at an angle consistent with its nominal geometry, the inner most edge of the CDG

mirror where it is finished at a knife edge would have been more susceptible to the removal of material in the polishing process. This would effectively lower the CDG angle in the areas closest to the knife edge, which is the area that reflects the interfering light for the outermost area of the resulting SRGs. It is believed that the higher than expected grating pitches from the outside few points of the SRG measurements are indicative of a slight change of less than one degree in the CDG angle at the inside edge of the CDG mirror. This accidental discovery may actually be beneficial in that it shows the potential for further controlling the rate of pitch by manipulating the curvature of the CDG mirrors.

After the accuracy of the simulation had been independently confirmed by comparing it to the experimental data, further simulations were run in order to demonstrate the potential range of pitches and the degree of chirp. Similar geometry was chosen as used in the experiment. However, a wider range of values of s were used. The results of these simulation runs are summarized in Figure 5.16. This graph demonstrates that by using small positive values of s, it is possible to achieve grating pitches smaller than the wavelength of light. This overcomes the theoretical limit of minimum pitch for circular SRG production using a collimated light source with a CDG as seen in equation (3.4.11). For small positive or negative values of s, the change in grating pitch, or chirp is most pronounced. Maximum values for grating chirp rate measured from the bottom and top curves in Figure 5.16 are -30.1 nm pitch/mm and 34.1 nm pitch/mm for values of s = 1 cm and s = -2 cm respectively.

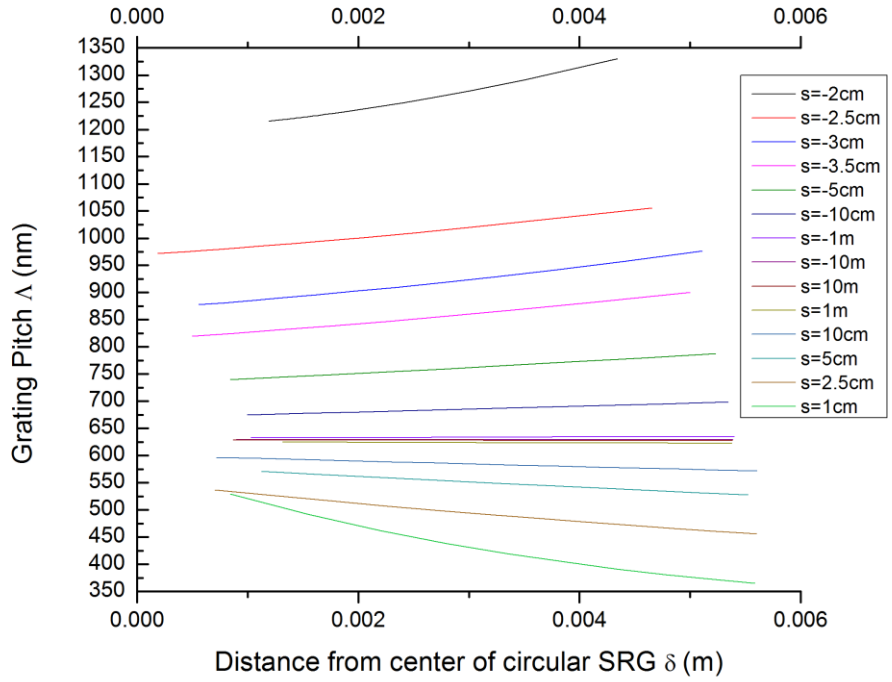

Figure 5.16 - The dependence of grating pitch on distance from the center of the grating for 14 simulated circular SRGs inscribed with a 28.9 degrees CDG using different distances to the point source of light, s, with a wavelength of 532 nm. A positive value of s denotes divergent source while a negative value indicates a convergent source. As the distance to the point source increases, whether positive or negative, the slope of the grating pitch over distance from centre of SRG approaches zero. Small absolute values of s result in steeper slopes and nonlinear curves. The grating pitch can be further controlled by changing the CDG angle θ or the wavelength of light λ. Curves are derived from a ray trace computer simulation discussed in theory section of this thesis and seen in Appendix A.

An additional result that can be seen in Figure 5.16 happens for very distant point sources. Whether converging or diverging, the curvature of the inscribing light becomes less pronounced at far distances to the source and is a closer approximation to collimated light. For values of s=10 m or s=-10m, the slope of the curves generated approaches zero. This is consistent with the constant pitch gratings generated in the collimated beam experiment. The values of pitch for distant point sources in Figure 5.16 are consistent with the predicted pitch from equation (3.4.11) for an SRG inscribed using a 28.9 degree CDG with 532 nm wavelength collimated beam. Both results independently arrive at a constant pitch value of approximately 629 nm. This shows that the derived theory for the chirped pitch circular gratings is simply a more general case of the theory that was developed for the constant pitch gratings, and that the two theoretical solutions are in agreement.

CHAPTER 6: CONCLUSION

This thesis has introduced a novel holographic method of generating circular diffraction gratings using a specially designed mirror fixture called a Circular Diffraction Grating Generator (CDG). The circular gratings are inscribed in surface relief on thin films of photo-mechanically active azo-glass material. The theory describing the geometry of interfering light reflected by the CDG has been developed in order to predict the grating pitch as well as the rate of grating chirp for circular surface relief gratings (SRGs) fabricated by this method. A ray trace simulation was used as a tool to model the pitch of the generated SRGs and the results from this simulation agreed well with the theory as well as the experimental data.

A collimated beam of coherent light can be used to create constant pitch circular SRGs. By focusing the inscribing light to a point source, either converging or diverging on the CDG mirror, it is possible to create chirped circular SRGs with positive or negative rates of changes in pitch over the surface of the grating. The result is that the pitch and chirp of the circular gratings can be controlled with a relatively high degree of accuracy within the confines of the theory by changing the geometry of the experiment and the wavelength of the inscribing light.

One of the main advantages to this method of fabricating circular SRGs is the speed that the gratings are produced. While other methods of fabrication such as grating engines, or direct milling with energy beams can produce gratings with comparable resolutions, it can take days of milling one groove at a time on expensive machinery to produce a grating of a few centimeters across. Photolithography can produce gratings much more quickly than direct milling, but still requires the fabrication of a photo mask. The method of creating circular SRGs outlined in this thesis can be described as a form of direct 3D interference photolithography, which combines the advantages of photolithography without the requirement for a photo-mask or chemical etching. The result is a single step process that can create holographic circular gratings quickly, without the requirement for a master grating or photo-mask, and without any specialized equipment other than a suitably powerful laser. In the case of the experiments outlined in this thesis, good quality gratings were formed in 350 seconds using a beam irradiance of 604 mW/cm^2. Less powerful inscribing sources of around 100 mW/cm^2 would also work, but would require more exposure time.

Another advantage of this circular SRG manufacturing technique is the relatively large scale of the gratings produced while still maintaining very fine sub micrometer detail in the grating structure. While other methods of direct inscription of circular gratings in azo-polymer films have been demonstrated, the size of these gratings has been in the order of micrometers. It has been demonstrated in this thesis that by using a CDG, it is possible to fabricate circular SRGs more than a centimeter across while maintaining a diffraction grating structure finer than 500 nm. This method can be similarly scaled up or scaled down to meet application specific requirements by changing the size of the CDG. The main practical limit to the size of a circular SRGs produced by this method is the irradiance of the collimated beam from the inscribing laser which must be wide enough to illuminate the entire CDG and also have enough power to activate the photo-mechanical response in the azo-material film with an irradiance of at least 50 mW/cm^2 as discussed in section 1.4.

An interesting result from the analysis of the theory and experiments is the fact that the circular SRGs created by this new holographic method are very sensitive to the height of the CDG. It is important that its height not exceed the 'critical height' of the CDG or else the interfering beams will cross over the centre point of the circular grating and cause an unwanted third source of interference. However, if the height of the CDG is less than the critical height, then it is possible to create a ring diffraction grating. The ability to create ringed gratings may serve as an advantage in certain applications where the gratings serve to focalize or couple light towards a sample material in the centre of the rings. Varying the height of the CDG below the critical height changes the thickness of the ring grating and allows for an additional element of controllability in the fabrication of gratings by this method.

Areas of future development on the topic of holographic circular gratings should concentrate on application based research. Researchers using circular diffraction gratings in their work may benefit greatly from the ability to create customized circular SRGs with the required size and pitch in a fast, single-step process. Because of the relative simplicity of this manufacturing process without the requirement for specialized complex equipment, this technology may enable small laboratories to fabricate their own customized circular gratings in order to further application based research in their own fields. It is anticipated that areas of research such as diffractive lenses, surface emitting feedback dye lasers, and plasmonic enhancement of LEDs or solar cells, will now be more accessible to research groups that

previously did not previously have the ability to manufacture their own circular gratings in house, thus paving the way for future discoveries in the field of photonics.

References

[1] Magnusson, R. and Gaylord, T. , "Diffraction efficiencies of thin phase gratings with arbitrary grating shape," J.Opt.Soc.Am. 68(6), 806-809 (1978).

[2] Gregory, J. , "Letter from James Gregory to John Collins dated 13 May 16y3,", 251-255-254 (1841).

[3] Hopkinson, F. and Rittenhouse, D. , "An optical problem, proposed by Mr. Hopkinson, and solved by Mr. Rittenhouse," Transactions of the American Philosophical Society 2, 201-206 (1786).

[4] Fraunhofer, J. , "New modification of light by the mutual influence and the diffraction of [light] rays, and the laws thereof," Memoirs of the Royal Academy of Science in Munich 8, 3-76 (1821).

[5] Rayleigh, John William Strutt Baron, [Scientific Papers: 1887-1892], University Press (1902).

[6] Wood, R. W. , "Phase-Reversal Zone Plate and Diffraction Telescopes," Philosophical Magazine, fifth series 45(277), 511-523 (1898).

[7] Tiwari, U., Tripathi, S. M., Thyagarajan, K., Shenoy, M. R., Mishra, V., Jain, S. C., Singh, N. and Kapur, P. , "Tunable wavelength division multiplexing channel isolation filter based on dual chirped long-period fiber gratings," Opt.Lett. 36(19), 3747-3749 (2011).

[8] Schasfoort, R. B. M. and Tudos, A. J. , "Handbook of Surface Plasmon Resonance," (2008).

[9] Wikipedia contributors , "Azobenzene," 2014(25 September) (2014).

[10] Rochon, P., Batalla, E. and Natansohn, A. , "Optically induced surface gratings on azoaromatic polymer films," Appl.Phys.Lett. 66(2), 136-138 (1995).

[11] Kim, D., Tripathy, S., Li, L. and Kumar, J. , "Laser-induced holographic surface relief gratings on nonlinear optical polymer films," Appl.Phys.Lett. 66(10), 1166-1168 (1995).

[12] Viswanathan, N., Kim, D. and Tripathy, S. , "Surface relief structures on azo polymer films," Journal of Materials Chemistry 9(9), 1941-1955 (1999).

[13] Kirby, R., Sabat, R. G., Nunzi, J. and Lebel, O. , "Disperse and disordered: a mexylaminotriazine-substituted azobenzene derivative with superior glass and surface relief grating formation," J.Mater.Chem.C 2(5), 841-847 (2014).

[14] Yi, J., Biao, C. and Changan, Z., "Design, analysis and control of a precision feeding system of diffraction grating ruling engine," Advanced Intelligent Mechatronics (AIM), 2012 IEEE/ASME International Conference on, 160-165 (2012).

[15] Vieu, C., Carcenac, F., Pepin, A., Chen, Y., Mejias, M., Lebib, A., Manin-Ferlazzo, L., Couraud, L. and Launois, H. , "Electron beam lithography: resolution limits and applications," Appl.Surf.Sci. 164(1), 111-117 (2000).

[16] Moss, D., Ta'eed, V., Eggleton, B., Freeman, D., Madden, S., Samoc, M., Luther-Davies, B., Janz, S. and Xu, D. , "Bragg gratings in silicon-on-insulator waveguides by focused ion beam milling," Appl.Phys.Lett. 85(21), 4860-4862 (2004).

[17] Shah, L., Fermann, M. E., Dawson, J. W. and Barty, C. P. , "Micromachining with a 50 W, 50 μJ, subpicosecond fiber laser system," Optics express 14(25), 12546-12551 (2006).

[18] Singh, S. , "Diffraction gratings: aberrations and applications," Optics & Laser Technology 31(3), 195-218 (1999).

[19] Päivänranta, B., Langner, A., Kirk, E., David, C. and Ekinci, Y. , "Sub-10 nm patterning using EUV interference lithography," Nanotechnology 22(37), 375302 (2011).

[20] Yang, C., Shi, K., Edwards, P. and Liu, Z. , "Demonstration of a PDMS based hybrid grating and Fresnel lens (G-Fresnel) device," Optics express 18(23), 23529-23534 (2010).

[21] Xia, Y., Kim, E., Zhao, X. M., Rogers, J. A., Prentiss, M. and Whitesides, G. M. , "Complex Optical Surfaces Formed by Replica Molding Against Elastomeric Masters," Science 273(5273), 347-349 (1996).

[22] Lasagni, A. , Acevedo, D. , Barbero, C. and Mücklich, F. , "One-Step Production of Organized Surface Architectures on Polymeric Materials by Direct Laser Interference Patterning," Advanced Engineering Materials 9(1-2), 99-103 (2007).

[23] Bremus-Koebberling, E. A., Beckemper, S., Koch, B. and Gillner, A. , "Nano structures via laser interference patterning for guided cell growth of neuronal cells," J.Laser Appl. 24(4), 042013 (2012).

[24] Priimagi, A. and Shevchenko, A. , "Azopolymer-based micro- and nanopatterning for photonic applications," Journal of Polymer Science Part B: Polymer Physics 52(3), 163-182 (2014).

[25] Grosjean, T. and Courjon, D. , "Photopolymers as vectorial sensors of the electric field," Opt.Express 14(6), 2203-2210 (2006).

[26] Kim, J. K., Jung, Y., Lee, B. H., Oh, K., Chun, C. and Kim, D. , "Optical phase-front inscription over optical fiber end for flexible control of beam propagation and beam pattern in free space," Optical Fiber Technology 13(3), 240 (2007).

[27] Buralli, D. A., Morris, G. M. and Rogers, J. R. , "Optical performance of holographic kinoforms," Appl.Opt. 28(5), 976-983 (1989).

[28] Khonina, S. N., Ustinov, A. V. and Volotovsky, S. G. , "Fractional axicon as a new type of diffractive optical element with conical focal region," Precision Instrument and Mechanology 2(4), 132-143 (2013).

[29] He, P., Wang, F., Li, L., Georgiadis, K., Dambon, O., Klocke, F. and Yi, A. , "Development of a low cost high precision fabrication process for glass hybrid aspherical diffractive lenses," Journal of Optics 13(8), 085703 (2011).

[30] Bhat, R. D., Panoiu, N. C., Brueck, S. R. and Osgood, R. M. , "Enhancing the signal-to-noise ratio of an infrared photodetector with a circular metal grating," Opt.Express 16(7), 4588-4596 (2008).

[31] Toma, K., Vala, M., Adam, P., Homola, J., Knoll, W. and Dostálek, J. , "Compact surface plasmon-enhanced fluorescence biochip," Optics express 21(8), 10121-10132 (2013).

[32] Park, Y. and Choi, S. H. , "Miniaturization of optical spectroscopes into Fresnel microspectrometers," Journal of Nanophotonics 7(1), 077599-077599 (2013).

[33] Shang, H. M., Toh, S. L., Fu, Y., Quan, C. and Tay, C. J. , "The use of circular optical grating for measuring angular rotation of mirrors," Optics and Lasers in Engineering 36(5), 487 (2001).

[34] Olson, C. and Hall, D. G. , "Azimuthal mode discrimination in radially chirped concentric-circle-grating distributed feedback lasers," Quantum Electronics, IEEE Journal of 36(9), 1016-1025 (2000).

[35] Chen, Y., Li, Z., Zhang, Z., Psaltis, D. and Scherer, A. , "Nanoimprinted circular grating distributed feedback dye laser," Appl.Phys.Lett. 91(5), 051109 (2007).

[36] Zhu, J., Zhang, H., Zhu, Z., Li, Q. and Jin, G. , "Surface-plasmon-enhanced GaN-LED based on the multilayered rectangular nano-grating," Opt.Commun. 322(0), 66 (2014).

[37] Vuckovic, J., Loncar, M. and Scherer, A. , "Surface plasmon enhanced light-emitting diode," Quantum Electronics, IEEE Journal of 36(10), 1131-1144 (2000).

[38] Janjua, B. and Jabbour, G., "Broadband back grating design for thin film solar cells," Photonics Conference (IPC), 2013 IEEE, 578-579 (2013).

[39] Pala, R. A., White, J., Barnard, E., Liu, J. and Brongersma, M. L. , "Design of Plasmonic Thin-Film Solar Cells with Broadband Absorption Enhancements," Adv Mater 21(34), 3504-3509 (2009).

[40] Rastani, K., Marrakchi, A., Habiby, S. F., Hubbard, W. M., Gilchrist, H. and Nahory, R. E. , "Binary phase Fresnel lenses for generation of two-dimensional beam arrays," Appl.Opt. 30(11), 1347-1354 (1991).

[41] Hecht, E., [Optics], Pearson - Addison Wesley, San Fransisco (2002).

Appendix A: Code for ray trace simulation of CDG with converging and diverging wavefronts

```
clearvars
close all
format long
syms theta
d=5.95e-3; %set radius of minor aperture (m)
theta=28.9; % set CDG angle (degrees)
s=-100e-3; % set distanc to point source (m)
lambda=532e-9; % set wavelength of inscribing light (m)
%h=d/(tand(2*theta)-tand(theta))*.397
h=7.99e-3; % set height of CDG
t=h*tand(theta); % calculate thickness of CDG based on height and angle

%angle of reflection calculations in matrix form
%mirror=[d 0 d+t h]
%beam1=[d; -s]
%beam2=[d+t; h-s]
%reflectionmatrix=[cosd(-theta)     -sind(-theta);sind(-theta)     cosd(-
theta)]*[-1 0;0 1]*[cosd(theta) -sind(theta);sind(theta) cosd(theta)]
%reflection1=reflectionmatrix*beam1

angleout1=atand(d/s);  %calculate  the  angle  from  the  point  source  to
innermost point on the CDG mirror
angleout2=abs(atand((d+t)/(s-h)));  % calculate the angle from the point
source to the outermost point on the CDG mirror

%calculate  the  reflected  angle  from  the  CDG  mirror  for  the  two  beams
above
if s>0
       reflectedangle1=(angleout1+2*theta);
    reflectedangle2=(angleout2+2*theta);
 else
     reflectedangle1=(-angleout1+2*theta);
    reflectedangle2=(-angleout2+2*theta);
 end

counter=0;
scanincrement=.5e-3; %set the sample rate for how many test points you'd
like (m)
%scan and calculate test points to use
for   x=d+scanincrement:scanincrement:d+t   %loop   in   increments   of
scanincrement along the length of the CDG mirror
    counter=counter+1;
    y=(x-d)/tand(theta);   % calculate the y position on the CDG mirror
where the beam will hit
    angleout=abs(atand(x/(s-y)));  % calculate the angle from the source
in order to hit the test point on the CDG mirror
```

```
    %calculate the reflected angle for the test point on the CDG mirror
    if s>0
        reflectedangle=(angleout+2*theta);
    else
        reflectedangle=(-angleout+2*theta);
    end

    finalx=x-y*tand(reflectedangle);% calculate the final x coord at
sample after reflection

    %draw the ray trace lines on the schematic
    incident=line([0 x],[s y],'Color', [0 1 0]);
    reflected=line([x finalx],[y 0],'Color', [0 1 0]);
    straightin=line([0 finalx],[s 0],'Color', [0 0 1]);

    %this section of code estimates the grating pitch by calculating the
    %path difference between the test points selected above, and by
moving
    %in small increments away from the test point until a differnce in
path
    %difference of one wavelength is found

    %calculate the pathdifference between incident and reflected beams
for the test point
    if s>0
        pathdifference=sqrt(x^2+(y-s)^2)+sqrt((x-finalx)^2+y^2)-
sqrt(finalx^2+s^2);
    else
        pathdifference=-sqrt(x^2+(y-s)^2)+sqrt((x-
finalx)^2+y^2)+sqrt(finalx^2+s^2);
    end
    pdinwavelengths=pathdifference/lambda; % convert from m to # of
wavelengths

    phasescan=0;
    microincrement=1e-10; %set very small incremental increase parameter
    scanposition=x;
    while phasescan<1 % loop while the difference between path difference
is less then one wavelength
        scanposition=scanposition+microincrement; %increase the scan
position by one scan increment
        y=(scanposition-d)/tand(theta); % calculate the y position on the
mirror where the scan will strike
        angleout=abs(atand(scanposition/(s-y))); % calculate the angle
from the point source to hit the scan position on mirror

        %calculate the reflected angle of the scan
        if s>0
            reflectedangle=(angleout+2*theta);
         else
            reflectedangle=(-angleout+2*theta);
        end
```

```
        finalxscan=scanposition-y*tand(reflectedangle);  % calculate the
xposition on the sample where the reflected scan ray will hit

        %calculate the path difference between incident and reflected
light
        %for the scan position
        if s>0
            pathdifference=sqrt(scanposition^2+(y-
s)^2)+sqrt((scanposition-finalxscan)^2+y^2)-sqrt(finalxscan^2+s^2);
        else
            pathdifference=-sqrt(scanposition^2+(y-
s)^2)+sqrt((scanposition-finalxscan)^2+y^2)+sqrt(finalxscan^2+s^2);
        end
        micropdinwavelengths=pathdifference/lambda;    %    convert    scan
position PD from m to # of wavelengths
        phasescan=abs(pdinwavelengths-micropdinwavelengths);        %check
difference between path length between test point and scan point
    end

   %store position in x direction of test point and the resulting
   %calculated pitch in two arrays
   position(counter)=finalx;
   pitch(counter)=(finalx-finalxscan);

end
%output the position and calculate pitch
position.'
pitch.'

%draw remainder of elements on ray trace schematic
scrsz=get(0,'ScreenSize');
%figure('Name','CDG   simulation',   'NumberTitle',   'on',   'Position',[1
scrsz(4)/2 scrsz(3)/2 scrsz(4)/2])
axis([0 d+t 0 .01])
axis equal
%draw mirror
mirror=line([d d+t],[0 h]);
%draw inside border line
incident1=line([0 d],[s 0], 'Color', [1 0 0]);
%draw outside border line
incident2=line([0 d+t],[s h], 'Color', [1 0 0]);
reflected2=line([d+t  d+t-h*tand(reflectedangle2)],[h  0],'Color',  [1  0
0]);

%plot position vs pitch graph
figure
plot(position,pitch)
%position
%pitch
```

Appendix B: Papers published or under review from research

Leibold, J., Snell, P., Lebel, O., and Sabat, R.G. "Design and fabrication of constant-pitch circular surface-relief diffraction gratings on disperse red 1 glass". Opt. Lett. 2014, 39, 3445-3448.

Leibold, J. and Sabat, R.G. "Laser-induced Controllable Chirped-Pitch Circular Surface-Relief Diffraction Gratings on Azo-Glass" Under review in Photonics Research as of Mar 2015.